

Rethinking Robustness of Model Attributions

Sandesh Kamath¹, Sankalp Mittal¹, Amit Deshpande², Vineeth N Balasubramanian¹

¹Indian Institute of Technology, Hyderabad

²Microsoft Research, Bengaluru
sandesh.kamath@gmail.com,

Abstract

For machine learning models to be reliable and trustworthy, their decisions must be interpretable. As these models find increasing use in safety-critical applications, it is important that not just the model predictions but also their explanations (as feature attributions) be robust to small human-imperceptible input perturbations. Recent works have shown that many attribution methods are fragile and have proposed improvements in either these methods or the model training. We observe two main causes for fragile attributions: first, the existing metrics of robustness (e.g., top- k intersection) overpenalize even reasonable local shifts in attribution, thereby making random perturbations to appear as a strong attack, and second, the attribution can be concentrated in a small region even when there are multiple important parts in an image. To rectify this, we propose simple ways to strengthen existing metrics and attribution methods that incorporate locality of pixels in robustness metrics and diversity of pixel locations in attributions. Towards the role of model training in attributional robustness, we empirically observe that adversarially trained models have more robust attributions on smaller datasets, however, this advantage disappears in larger datasets. Code is made available¹.

1 Introduction

The explosive increase in the use of deep neural network (DNN)-based models for applications across domains has resulted in a very strong need to find ways to interpret the decisions made by these models (Gade et al. 2020; Tang et al. 2021; Yap et al. 2021; Oviedo et al. 2022; Oh and Jeong 2020). Interpretability is an important aspect of responsible and trustworthy AI, and model explanation methods (also known as attribution methods) are an important aspect of the community’s efforts towards explaining and debugging real-world AI/ML systems. Attribution methods (Zeiler et al. 2010; Simonyan, Vedaldi, and Zisserman 2014; Bach et al. 2015; Selvaraju et al. 2017; Chattopadhyay et al. 2018; Sundararajan, Taly, and Yan 2017; Shrikumar et al. 2016; Smilkov et al. 2017; Lundberg and Lee 2017) attempt to explain the decisions made by DNN models through input-output attributions or saliency maps. (Lipton 2018; Samek et al. 2019; Fan et al. 2021; Zhang et al. 2020) present detailed surveys on these methods. Recently, the growing

numbers of attribution methods has led to a concerted focus on studying the robustness of attributions to input perturbations to handle potential security hazards (Chen et al. 2019; Sarkar, Sarkar, and Balasubramanian 2021; Wang and Kong 2022; Agarwal et al. 2022). One could view these efforts as akin to adversarial robustness that focuses on defending against attacks on model predictions, whereas *attributional robustness* focuses on defending against attacks on model explanations. For example, an explanation for a predicted credit card failure cannot change significantly for a small human-imperceptible change in input features, or the saliency maps explaining the COVID risk prediction from a chest X-ray should not change significantly with a minor human-imperceptible change in the image.

DNN-based models are known to have a vulnerability to imperceptible adversarial perturbations (Biggio et al. 2013; Szegedy et al. 2014; Goodfellow, Shlens, and Szegedy 2015), which make them misclassify input images. Adversarial training (Madry et al. 2018) is widely understood to provide a reasonable degree of robustness to such perturbation attacks. While adversarial robustness has received significant attention over the last few years (Ozdag 2018; Silva and Najafirad 2020), the need for stable and robust attributions, corresponding explanation methods and their awareness are still in their early stages at this time (Ghorbani, Abid, and Zou 2019; Chen et al. 2019; Slack et al. 2020; Sarkar, Sarkar, and Balasubramanian 2021; Lakkaraju, Arsov, and Bastani 2020; Slack et al. 2021a,b). In an early effort, (Ghorbani, Abid, and Zou 2019) provided a method to construct a small imperceptible perturbation which when added to an input x results in a change in attribution map of the original map to that of the perturbed image. This is measured through top- k intersection, Spearman’s rank-order correlation or Kendall’s rank-order correlation between the two attribution maps (of original and perturbed images). See Figure 1 for an example. Defenses proposed against such attributional attacks (Chen et al. 2019; Singh et al. 2020; Wang et al. 2020; Sarkar, Sarkar, and Balasubramanian 2021) also leverage the same metrics to evaluate the robustness of attribution methods.

While these efforts have showcased the need and importance of studying the robustness of attribution methods, we note in this work that the metrics used, and hence the methods, can be highly sensitive to minor local changes in attribu-

¹<https://github.com/ksandeshk/LENS>



Figure 1: Sample images from Flower dataset with Integrated Gradients (IG) before and after attributional attack. The attack used here is the top- k attributional attack of Ghorbani, Abid, and Zou (2019) on a ResNet model. Robustness of attribution measured by top- k intersection is small, and ranges from 0.04 (first image) to 0.45 (third image) as it penalizes for both local changes in attribution and concentration of top pixels in a small region. Visually, we can observe that such overpenalization leads to a wrong sense of robustness as the changes are within the object of importance.

tions (see Fig 1 row 2). We, in fact, show (in Appendix B.1) that under existing metrics to evaluate robustness of attributions, a random perturbation can be as strong an attributional attack as existing benchmark methods. This may not be a true indicator of the robustness of a model’s attributions, and can mislead further research efforts in the community. We hence focus our efforts in this work on rethinking metrics and methods to study the robustness of model attributions (in particular, we study image-based attribution methods to have a focused discussion and analysis). Beyond highlighting this important issue, we propose locality-sensitive improvements of the above metrics that incorporate the locality of attributions along with their rank order. We show that such a locality-sensitive distance is upper-bounded by a metric based on symmetric set difference. We also introduce a new measure **top- k -div** that incorporates diversity of a model’s attributions. Our key contributions are summarized below:

- Firstly, we observe that existing robustness metrics for model attributions overpenalize minor drifts in attribution, leading to a false sense of fragility.
- In order to address this issue, we propose Locality-sensitive (LENS) improvements of existing metrics, namely, LENS-top- k , LENS-Spearman and LENS-Kendall, that incorporate the locality of attributions along

with their rank order. Besides avoiding overpenalizing attribution methods for minor local drifts, we show that our proposed LENS variants are well-motivated by metrics defined on the space of attributions.

- We subsequently introduce a second measure based on diversity that enriches model attributions by preventing the localized grouping of top model attributions. LENS can be naturally applied to this measure, thereby giving a method to incorporate both diversity and locality in measuring attributional robustness.
- Our comprehensive empirical results on benchmark datasets and models used in existing work clearly support our aforementioned observations, as well as the need to rethink the evaluation of the robustness of model attributions using locality and diversity.
- Finally, we also show that existing methods for robust attributions implicitly support such a locality-sensitive metric for evaluating progress in the field.

2 Background and Related Work

We herein discuss background literature from three different perspectives that may be related to our work: model explanation/attribution methods, efforts on attributional robustness (both attacks and defenses), and other recent related work. **Attribution Methods.** Existing efforts on explainability in DNN models can be broadly categorized as: local and global methods, model-agnostic and model-specific methods, or as post-hoc and ante-hoc (intrinsically interpretable) methods (Molnar 2019; Lecue et al. 2021). Most existing methods in use today – including methods to visualize weights and neurons (Simonyan, Vedaldi, and Zisserman 2014; Zeiler and Fergus 2014), guided backpropagation (Springenberg et al. 2015), CAM (Zhou et al. 2016), GradCAM (Selvaraju et al. 2017), Grad-CAM++ (Chattopadhyay et al. 2018), LIME (Ribeiro, Singh, and Guestrin 2016), DeepLIFT (Shrikumar et al. 2016; Shrikumar, Greenside, and Kundaje 2017), LRP (Bach et al. 2015), Integrated Gradients (Sundararajan, Taly, and Yan 2017), SmoothGrad (Smilkov et al. 2017)), DeepSHAP (Lundberg and Lee 2017) and TCAV (Kim et al. 2018) – are post-hoc methods, which are used on top of a pre-trained DNN model to explain its predictions. We focus on such post-hoc attribution methods in this work. For a more detailed survey of explainability methods for DNN models, please see (Lecue et al. 2021; Molnar 2019; Samek et al. 2019).

Robustness of Attributions. The growing numbers of attribution methods proposed has also led to efforts on identifying the desirable characteristics of such methods (Alvarez-Melis and Jaakkola 2018; Adebayo et al. 2018; Yeh et al. 2019; Chalasani et al. 2020; Tomsett et al. 2020; Boggust et al. 2022; Agarwal et al. 2022). A key desired trait that has been highlighted by many of these efforts is robustness or stability of attributions, i.e., the explanation should not vary significantly within a small local neighborhood of the input (Alvarez-Melis and Jaakkola 2018; Chalasani et al. 2020). Ghorbani, Abid, and Zou (2019) showed that well-known methods such as gradient-based attributions, DeepLIFT (Shrikumar, Greenside, and Kundaje

2017) and Integrated Gradients (IG) (Sundararajan, Taly, and Yan 2017) are vulnerable to such input perturbations, and also provided an algorithm to construct a small imperceptible perturbation which when added to the input results in changes in the attribution. Slack et al. (2020) later showed that methods like LIME (Ribeiro, Singh, and Guestrin 2016) and DeepSHAP (Lundberg and Lee 2017) are also vulnerable to such manipulations. The identification of such vulnerability and potential for attributional attacks has since led to multiple research efforts to make a model’s attributions robust. Chen et al. (2019) proposed a regularization-based approach, where an explicit regularizer term is added to the loss function to maintain the model gradient across input (IG, in particular) while training the DNN model. This was subsequently extended by (Sarkar, Sarkar, and Balasubramanian 2021; Singh et al. 2020; Wang et al. 2020), all of whom provide different training strategies and regularizers to improve attributional robustness of models. Each of these methods including Ghorbani, Abid, and Zou (2019) measures change in attribution before and after input perturbation using the same metrics: top- k intersection, and/or rank correlations like Spearman’s ρ and Kendall’s τ . Such metrics have recently, in fact, further been used to understand issues surrounding attributional robustness (Wang and Kong 2022). Other efforts that quantify stability of attributions in tabular data also use Euclidean distance (or its variants) between the original and perturbed attribution maps (Alvarez-Melis and Jaakkola 2018; Yeh et al. 2019; Agarwal et al. 2022). Each of these metrics look for dimension-wise correlation or pixel-level matching between attribution maps before and after perturbation, and thus penalize even a minor change in attribution (say, even by one pixel coordinate location). This results in a false sense of fragility, and could even be misleading. In this work, we highlight the need to revisit such metrics, and propose variants based on locality and diversity that can be easily integrated into existing metrics.

Other Related Work. In other related efforts that have studied similar properties of attribution-based explanations, (Carvalho, Pereira, and Cardoso 2019; Bhatt, Weller, and Moura 2020) stated that stable explanations should not vary too much between similar input samples, unless the model’s prediction changes drastically. The abovementioned attributional attacks and defense methods (Ghorbani, Abid, and Zou 2019; Sarkar, Sarkar, and Balasubramanian 2021; Singh et al. 2020; Wang et al. 2020) maintain this property, since they focus on input perturbations that change the attribution without changing the model prediction itself. Similarly, Arun et al. (2020) and Fel et al. (2022) introduced the notions of repeatability/reproducibility and generalizability respectively, both of which focus on the desired property that a trustworthy explanation must point to similar evidence across similar input images. In this work, we provide a practical metric to study this notion of similarity by considering locality-sensitive metrics.

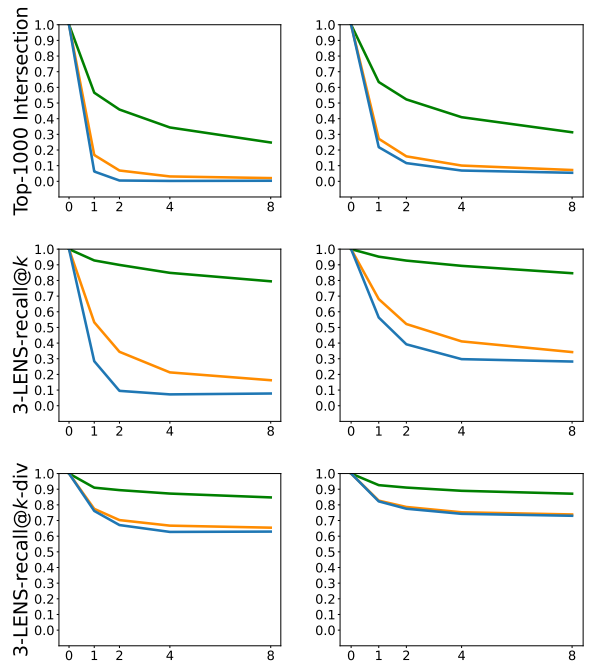


Figure 2: From top to bottom, we plot average top- k intersection (currently used metric), 3-LENS-recall@ k and 3-LENS-recall@ k -div (proposed metrics) against the ℓ_∞ -norm of attributional attack perturbations for Simple Gradients (SG) (left) and Integrated Gradients (IG) (right) of a SqueezeNet model on Imagenet. We use $k = 1000$ and three attributional attack variants proposed by Ghorbani, Abid, and Zou (2019). Evidently, the proposed metrics show more robustness under the same attacks.

3 Locality-sENSitive Metrics (LENS) for Attributional Robustness

As a motivating example, Figure 2 presents the results obtained using (Ghorbani, Abid, and Zou 2019) with Simple Gradients (SG) and Integrated Gradients (IG) of an NN model trained on ImageNet. The top row, which reports the currently followed top- k intersection measure of attribution robustness, shows a significant drop in robustness performance even for the random sign attack (green line). The subsequent rows, which report our metrics for the same experiments, show significant improvements in robustness – especially when combining the notions of locality and diversity. Observations made on current metrics could lead to a false sense of fragility, which overpenalizes even an attribution shift by 1-2 pixels. A detailed description of our experimental setup for these results is available in Appendix C. Motivated by these observations, we explore improved measures for attributional robustness that maintain the overall requirements of robustness, but do not overpenalize minor deviations.

3.1 Defining LENS Metrics for Attributions

To begin with, we propose an extension of existing similarity measures to incorporate the locality of pixel attribu-

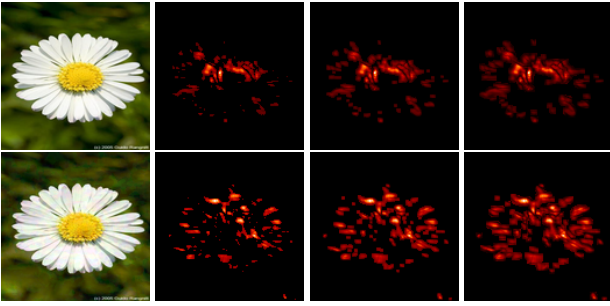


Figure 3: A sample image from Flower dataset before (top) and after (bottom) the top- k attributional attack of (Ghorbani, Abid, and Zou 2019) on a ResNet model for Integrated Gradients (IG) attribution method. From left to right: the image, its top- k pixels as per IG, the union of the 3×3 -pixel neighborhoods and 5×5 -pixel neighborhoods of the top- k pixels, respectively, for $k = 1000$. Quantitatively, top- k intersection: 0.14, 1-LENS-recall@ k : 0.25, 1-LENS-pre@ k : 0.37, 2-LENS-recall@ k : 0.40, 2-LENS-pre@ k : 0.62.

tions in images to derive more practical and useful measures of attributional robustness. Let $a_{ij}(x)$ denote the attribution value or importance assigned to the (i, j) -th pixel in an input image x , and let $S_k(x)$ denote the set of k pixel positions with the largest attribution values. Let $N_w(i, j) = \{(p, q) : i - w \leq p \leq i + w, j - w \leq q \leq j + w\}$ be the neighboring pixel positions within a $(2w + 1) \times (2w + 1)$ window around the (i, j) -th pixel. By a slight abuse of notation, we use $N_w(S_k(x))$ to denote $\bigcup_{(i,j) \in S_k(x)} N_w(i, j)$, that is, the set of all pixel positions that lie in the union of $(2w + 1) \times (2w + 1)$ windows around the top- k pixels.

For a given attributional perturbation $\text{Att}(\cdot)$, let $T_k = S_k(x + \text{Att}(x))$ denote the top- k pixels in attribution values after applying the attributional perturbation $\text{Att}(x)$. The currently used top- k intersection metric is then computed as: $|S_k(x) \cap T_k(x)|/k$. To address the abovementioned issues, we instead propose *Locality-sENSitive top- k metrics* (LENS-top- k) as $|N_w(S_k(x)) \cap T_k(x)|/k$ and $|S_k(x) \cap N_w(T_k(x))|/k$, which are also closer to more widely used metrics such as precision and recall in ranking methods. We similarly define *Locality-sENSitive Spearman's ρ* (LENS-Spearman) and *Locality-sENSitive Kendall's τ* (LENS-Kendall) metrics as rank correlation coefficients for the smoothed ranking orders according to $\tilde{a}_{ij}(x)$'s and $\tilde{a}_{ij}(x + \text{Att}(x))$'s, respectively. These can be used to compare two different attributions for the same image, the same attribution method on two different images, or even two different attributions on two different images, as long as the attribution vectors lie in the same space, e.g., images of the same dimensions where attributions assign importance values to pixels. Figure 3 provides the visualization of the explanation map of a sample from the Flower dataset with the top-1000 pixels followed by the corresponding maps with 1-LENS@ k and 2-LENS@ k .

We show that the proposed locality-sensitive variants of the robustness metrics also possess some theoretically

interesting properties. Let \mathbf{a}_1 and \mathbf{a}_2 be two attribution vectors for two images, and let S_k and T_k be the set of top k pixels in these images according to \mathbf{a}_1 and \mathbf{a}_2 , respectively. We define a locality-sensitive top- k distance between two attribution vectors \mathbf{a}_1 and \mathbf{a}_2 as $d_k^{(w)}(\mathbf{a}_1, \mathbf{a}_2) \stackrel{\text{def}}{=} \text{prec}_k^{(w)}(\mathbf{a}_1, \mathbf{a}_2) + \text{recall}_k^{(w)}(\mathbf{a}_1, \mathbf{a}_2)$, where $\text{prec}_k^{(w)}(\mathbf{a}_1, \mathbf{a}_2) \stackrel{\text{def}}{=} \frac{|S_k \setminus N_w(T_k)|}{k}$ and $\text{recall}_k^{(w)}(\mathbf{a}_1, \mathbf{a}_2) \stackrel{\text{def}}{=} \frac{|T_k \setminus N_w(S_k)|}{k}$, similar to precision and recall used in ranking literature, with the key difference being the inclusion of neighborhood items based on locality. Below we state a monotonicity property of $d_k^{(w)}(\mathbf{a}_1, \mathbf{a}_2)$ and upper bound it in terms of the symmetric set difference of top- k attributions.

Proposition 1. *For any $w_1 \leq w_2$, we have $d_k^{(w_2)}(\mathbf{a}_1, \mathbf{a}_2) \leq d_k^{(w_1)}(\mathbf{a}_1, \mathbf{a}_2) \leq |S_k \Delta T_k|/k$, where Δ denotes the symmetric set difference, i.e., $A \Delta B = (A \setminus B) \cup (B \setminus A)$.*

Combining $d_k^{(w)}(\mathbf{a}_1, \mathbf{a}_2)$ across different values of k and w , we can define a distance

$$d(\mathbf{a}_1, \mathbf{a}_2) = \sum_{k=1}^{\infty} \alpha_k \sum_{w=0}^{\infty} \beta_w d_k^{(w)}(\mathbf{a}_1, \mathbf{a}_2),$$

where α_k and β_w be non-negative weights, monotonically decreasing in k and w , respectively, such that $\sum_k \alpha_k < \infty$ and $\sum_w \beta_w < \infty$. We show that the distance defined above is upper-bounded by a metric similar to those proposed in (Fagin, Kumar, and Sivakumar 2003) based on symmetric set difference of top- k ranks to compare two rankings.

Proposition 2. *$d(\mathbf{a}_1, \mathbf{a}_2)$ defined above is upper-bounded by $u(\mathbf{a}_1, \mathbf{a}_2)$ given by*

$$u(\mathbf{a}_1, \mathbf{a}_2) = \sum_{k=1}^{\infty} \alpha_k \sum_{w=0}^{\infty} \beta_w \frac{|S_k \Delta T_k|}{k},$$

and $u(\mathbf{a}_1, \mathbf{a}_2)$ defines a bounded metric on the space of attribution vectors.

Note that top- k intersection, Spearman's ρ and Kendall's τ do not take the attribution values $a_{ij}(x)$'s into account but only the rank order of pixels according to these values. We also define a locality-sensitive w -smoothed attribution as follows.

$$\tilde{a}_{ij}^{(w)}(x) = \frac{1}{(2w + 1)^2} \sum_{\substack{(p,q) \in N_w(i,j), \\ 1 \leq p,q \leq n}} a_{pq}(x)$$

We show that the w -smoothed attribution leads to a contraction in the ℓ_2 norm commonly used in theoretical analysis of simple gradients as attributions.

Proposition 3. *For any inputs x, y and any $w \geq 0$, $\|\tilde{\mathbf{a}}^{(w)}(x) - \tilde{\mathbf{a}}^{(w)}(y)\|_2 \leq \|\mathbf{a}(x) - \mathbf{a}(y)\|_2$.*

Thus, any theoretical bounds on the attributional robustness of simple gradients in ℓ_2 norm proved in previous works continue to hold for locality-sensitive w -smoothed gradients. For example, (Wang et al. 2020) show the following Hessian-based bound on simple gradients. For an

input x and a classifier or model defined by f , let $\nabla_x(f)$ and $\nabla_y(f)$ be the simple gradients w.r.t. the inputs at x and y . Theorem 3 in (Wang et al. 2020) upper bounds the ℓ_2 distance between the simple gradients of nearby points $\|x - y\|_2 \leq \delta$ as $\|\nabla_x(f) - \nabla_y(f)\|_2 \lesssim \delta \lambda_{\max}(H_x(f))$, where $H_x(f)$ is the Hessian of f w.r.t. the input at x and $\lambda_{\max}(H_x(f))$ is its maximum eigenvalue. By Proposition 3 above, the same continues to hold for w -smoothed gradients, i.e., $\|\tilde{\nabla}_x^{(w)}(f) - \tilde{\nabla}_y^{(w)}(f)\|_2 \lesssim \delta \lambda_{\max}(H_x(f))$. The proofs of all the propositions above are included in Appendix D.

3.2 Relevance to Attributional Robustness

The top- k intersection is a measure of similarity instead of distance. Therefore, in our experiments for attributional robustness, we use locality-sensitive similarity measures w -LENS-prec@ k and w -LENS-recall@ k to denote $1 - \text{prec}_k^{(w)}(\mathbf{a}_1, \mathbf{a}_2)$ and $1 - \text{recall}_k^{(w)}(\mathbf{a}_1, \mathbf{a}_2)$, respectively, where \mathbf{a}_1 is the attribution of the original image and \mathbf{a}_2 is the attribution of the perturbed image. For rank correlation coefficients such as Kendall’s τ and Spearman’s ρ , we compute w -LENS-Kendall and w -LENS-Spearman as the same Kendall’s τ and Spearman’s ρ but computed on the locality-sensitive w -smoothed attribution map $\tilde{\mathbf{a}}^{(w)}$ instead of the original attribution map \mathbf{a} . We also study how these similarity measures and their resulting attributional robustness measures change as we vary w . In this section, we measure the attributional robustness of Integrated Gradients (IG) on naturally trained models as top- k intersection, w -LENS-prec@ k and w -LENS-recall@ k between the IG of the original images and the IG of their perturbations obtained by various attacks. The attacks we consider are the top- t attack and the mass-center attack of Ghorbani, Abid, and Zou (2019) as well as random perturbation. All perturbations have ℓ_∞ norm bounded by $\delta = 0.3$ for MNIST, $\delta = 0.1$ for Fashion MNIST, and $\delta = 8/255$ for GTSRB and Flower datasets.

The values of t used to construct top- t attacks of Ghorbani, Abid, and Zou (2019) are $t = 200$ on MNIST, $t = 100$ on Fashion MNIST and GTSRB, $t = 1000$ on Flower. In the robustness evaluations for a fixed k , we use $k = 100$ on MNIST, Fashion MNIST, GTSRB, and $k = 1000$ on Flower.

Comparison of top- k intersection, 1-LENS-prec@ k and 1-LENS-recall@ k . Figure 4 shows that top- k intersection penalizes IG even for small, local changes. 1-LENS-prec@ k and 1-LENS-recall@ k values are always higher in comparison across all datasets in our experiments. Moreover, on both MNIST and Fashion MNIST, 1-LENS-prec@ k is roughly 2x higher (above 90%) compared to top- k intersection (near 40%). In other words, an attack may appear stronger under a weaker measure of attributional robustness, if it ignores locality. This increase clearly shows that the top- k attack of Ghorbani, Abid, and Zou (2019) appears to be weaker on these datasets as the proportional increase by using locality indicates that the attack is only creating a local change than previously thought. We can see that for MNIST, Fashion-MNIST and GTSRB for $< 20\%$ of the samples, the top- k attack was able to make changes larger than what 1-LENS@ k could measure.

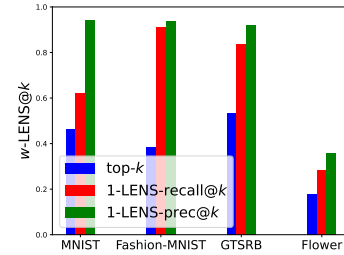


Figure 4: Attributional robustness of IG on naturally trained models measured as average top- k intersection, 1-LENS-prec@ k and 1-LENS-recall@ k between IG(original image) and IG(perturbed image) obtained by the top- t attack (Ghorbani, Abid, and Zou 2019) across different datasets.

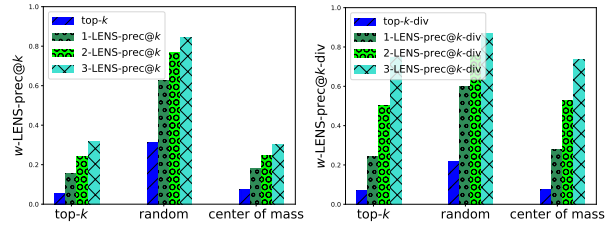


Figure 5: Effect of increasing w on average w -LENS-prec@ k and w -LENS-prec@ k -div in comparison with top- k intersection for IG map on ImageNet using a SqueezeNet model, when attacked with three attributional attacks (viz., top- k , random sign perturbation and mass center) of Ghorbani, Abid, and Zou (2019).

w -LENS-prec@ k for varying w . In Figure 5(left) w -LENS-prec@ k increases as we increase w to consider larger neighborhoods around the pixels with top attribution values. This holds for multiple perturbations, namely, top- t attack and mass-center attack by Ghorbani, Abid, and Zou (2019) as well as a random perturbation. Notice that the top- t attack of Ghorbani, Abid, and Zou (2019) is constructed specifically for the top- t intersection objective, and perhaps as a result, shows larger change when we increase local-sensitivity by increasing w in the robustness measure.

Due to space constraint and purposes of coherence, we present few results with IG here; we present similar results on other explanation methods in the Appendix E. Refer to Appendix E.2 for similar plots with random sign perturbation and mass center attack of Ghorbani, Abid, and Zou (2019). Appendix E.3 contains additional results with similar conclusions when Simple Gradients are used instead of Integrated Gradients (IG) for obtaining the attributions.

As a natural follow-up question we present in Appendix E.1 results obtained by modifying the similarity objective of top- k attack of Ghorbani, Abid, and Zou (2019) with 1-LENS-prec@ k with the assumption to obtain a stronger attack. But surprisingly, we notice that it leads to a *worse* attributional attack, if we measure its effectiveness using the top- k intersections and 1-LENS-prec@ k . In other words, attributional attacks against locality-sensitive measures of attributional robustness are non-trivial and may require funda-

mentally different ideas.

3.3 Alignment of attributional robustness metrics to human perception

We conducted a survey with human participants, where we presented images from the Flower dataset and a pair of attribution maps—an attribution map of the original image alongside an attribution map of their random perturbation or attributional attacked version Ghorbani, Abid, and Zou (2019), in a random order and without revealing this information to the participants. The survey participants were asked whether the two maps were relatable to the image and if one of them was different than the other. In Table 1 we summarize the results obtained from the survey. We simplify the choices presented to the user into 2 final categories - (1) Agree with w -LENS-prec@ k (2) Agree with top- k metric Category (1) includes all results where the user found the maps the same, relatable to the image but dissimilar or the perturbed map was preferred over the original map. Category (2) was the case where the user preferred the original map over the perturbed map. Refer to Appendix I for more details.

Agree with 3-LENS-prec@ k metric(%)	Agree with top- k metric(%)
70.37	29.63

Table 1: Survey results based on humans ability to relate the explanation map to the original image with or without noise using the Flower dataset.

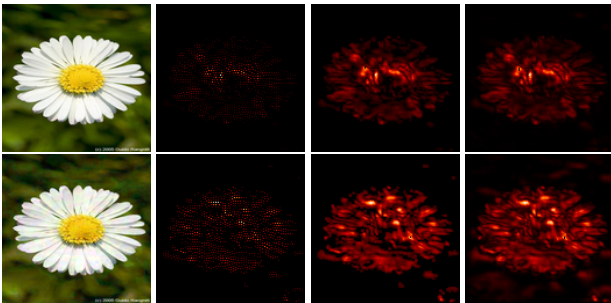


Figure 6: A sample image from Flower dataset before (top) and after (bottom) the top- k attributional attack of Ghorbani, Abid, and Zou (2019) on a ResNet model. For both, we show from left to right: the image, its top- k diverse pixels as per IG, the union of 3×3 -pixel neighborhoods and 5×5 -pixel neighborhoods of the top- k diverse pixels, respectively, for $k = 1000$. Quantitatively, improved overlap is captured by top- k -div intersection: 0.22, 1-LENS-recall@ k -div: 0.87, 1-LENS-pre@ k -div: 0.86, 2-LENS-recall@ k -div: 0.95, 2-LENS-pre@ k -div: 0.93. *Zoom in required to see the diverse pixels.*

4 Diverse Attribution for Robustness

Column 1 of Figure 6 shows a typical image from Flower dataset whose top-1000 pixels according to IG are concentrated in a small region. As seen in this illustrative exam-

ple, when an image has multiple important parts, concentration of top attribution pixels in a small region increases vulnerability to attributional attacks. To alleviate this vulnerability, we propose post-processing any given attribution method to output top- k diverse pixels instead of just the top- k pixels with the highest attribution scores. We use a natural notion of w -diversity based on pixel neighborhoods, so that these diverse pixels can be picked by a simple greedy algorithm. Starting with $S \leftarrow \emptyset$, repeat for k steps: Pick the pixel of highest attribution score or importance outside S , add it to S and disallow the $(2w + 1) \times (2w + 1)$ -pixel neighborhood around it for future selection. The set of k diverse pixels picked as above contains no two pixels within $(2w + 1) \times (2w + 1)$ -pixel neighborhood of each other, and moreover, has the highest total importance (as the sum of pixel-wise attribution scores) among all such sets of k pixels. The sets of k pixels where no two pixels lie in $(2w + 1) \times (2w + 1)$ -pixel neighborhood of each other form a matroid, where the optimality of greedy algorithm is well-known; see Korte and Lovász (1981).

Once we have the top- k diverse pixels as described above, we can extend our locality-sensitive robustness metrics from the previous section to w -LENS-prec@ k -div and w -LENS-recall@ k -div, defined analogously using the union of $(2w + 1) \times (2w + 1)$ -pixel neighborhoods of top- k diverse pixels. In other words, define $\tilde{S}_k(x)$ as the top- k diverse pixels for image x and $\tilde{T}_k = \tilde{S}_k(x + \text{Att}(x))$, and use \tilde{S}_k and \tilde{T}_k to replace S_k and T_k used in Subsection 3.1.

For $k = 1000$, Figure 6 shows a sample image from Flower dataset before and after the top- k attributional attack of Ghorbani, Abid, and Zou (2019). Figure 6 visually shows the top- k diverse pixels in the Integrated Gradients (IG) and the union of their $(2w + 1) \times (2w + 1)$ -pixel neighborhoods, for $w = \{1, 2\}$, for this image before and after the attributional attack. The reader may be required to zoom in to see the top- k diverse pixels. See Appendix F for more examples. Note that 0-LENS-prec@ k and 0-LENS-recall@ k are both the same and equivalent to top- k intersection. However, a combined effect of locality and diversity can show a drastic leap from top- k intersection value 0.14 to 2-LENS-recall@ k -div value 0.95 (see Fig.3 and Fig.6). Fig. 5(right) shows the effect of increasing w on the w -LENS-prec@ k -div metric on ImageNet.

5 A Stronger Model for Attributional Robustness

A common approach to get robust attributions is to keep the attribution method unchanged but train the models differently in a way that the resulting attributions are more robust to small perturbations of inputs. Chen et al. (2019) proposed the first defense against the attributional attack of Ghorbani, Abid, and Zou (2019). Wang et al. (2020) also find that IG-NORM based training of Chen et al. (2019) gives models that exhibit attributional robustness against the top- k attack of Ghorbani, Abid, and Zou (2019) along with adversarially trained models. Figure 7 shows a sample image from the Flower dataset, where the Integrated Gradients (IG) of the original image and its perturbation by the top- k attack are vi-

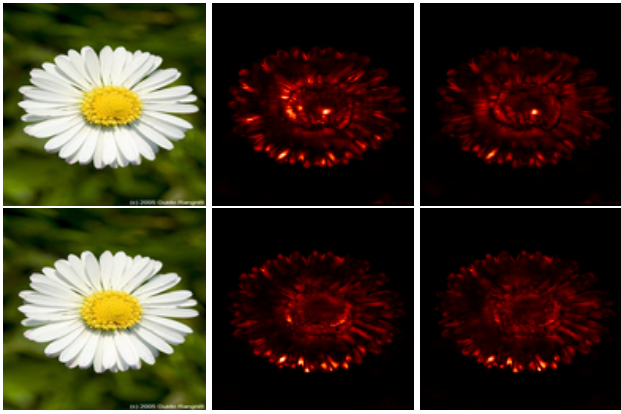


Figure 7: From left to right: a sample image from Flower dataset and Integrated Gradients (IG) before and after the top- k attributional attack of Ghorbani, Abid, and Zou (2019). The top row uses PGD-trained model whereas the bottom row uses IG-SUM-NORM-trained model.

sually similar for models that are either adversarially trained (trained using Projected Gradient Descent or PGD-trained, as proposed by (Madry et al. 2018)) or IG-SUM-NORM trained as in Chen et al. (2019). In other words, these differently trained model guard the sample image against the attributional top- k attack. Recent work by Norelahi et al. (2022) has empirically studied the effectiveness of adversarially (PGD) trained models in obtaining better attributions, e.g., Figure 7(center) shows sharper attributions to features highlighting the ground-truth class.

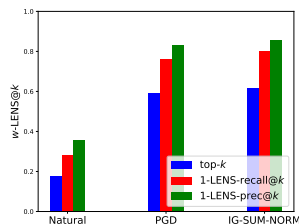


Figure 8: For Flower dataset, average top- k intersection, 1-LENS-prec@ k , 1-LENS-recall@ k measured between IG(original image) and IG(perturbed image) for models that are naturally trained, PGD-trained and IG-SUM-NORM trained. The perturbation used is the top- t attack of (Ghorbani, Abid, and Zou 2019). Note top- k is equivalent to 0-LENS-prec@ k , 0-LENS-recall@ k .

Figure 8 shows that PGD-trained and IG-SUM-NORM trained models have more robust Integrated Gradients (IG) in comparison to their naturally trained counterparts, and this holds for the previously used measures of attributional robustness (e.g., top- k intersection) as well as the new locality-sensitive measures we propose (e.g., 1-LENS-prec@ k , 1-LENS-recall@ k) across all datasets in Chen et al. (2019) experiments (Refer Appendix E.2 and E.3). The top- k attack of Ghorbani, Abid, and Zou (2019) is not a threat

to IG if we simply measure its effectiveness using 1-LENS-prec@ k (Appendix E.2, E.3 for MNIST, Fashion MNIST and GTSRB). The above observation about robustness of Integrated Gradients (IG) for PGD-trained and IG-SUM-NORM trained models holds even when we use 1-LENS-Spearman and 1-LENS-Kendall measures to quantify the attributional robustness to the top- k attack of Ghorbani, Abid, and Zou (2019), and it holds across the datasets used by Chen et al. (2019) in their study; see Appendix E.

Chalasanani et al. (2020) show theoretically that ℓ_∞ -adversarial training (PGD-training) leads to stable Integrated Gradients (IG) under ℓ_1 norm. They also show empirically that PGD-training leads to sparse attributions (IG & DeepSHAP) when sparseness is measured indirectly as the change in Gini index. Our empirical results extend their theoretical observation about stability of IG for PGD-trained models, as we measure local stability in terms of both the top attribution values and their positions in the image.

Table 2 obtains the top- k intersection, 3-LENS-recall@ k , and 3-LENS-recall@ k -div of different attribution methods on ImageNet for naturally trained and PGD-trained ResNet50 models. We observe that for random sign attack the improvement obtained on top- k intersection is reduced for a large dataset like ImageNet. Still our conclusions about locality and diversity in attribution robustness in comparison with the top- k intersection baseline holds as we observe improvements in using diversity and locality. More results about incorporating diversity in the attribution and the resulting robustness metrics are available in Appendix H.

Training	Attribution method	top- k	3-LENS-recall@ k	3-LENS-recall@ k -div
Natural	Simple Gradient	0.3825	0.7875	0.8290
Natural	Image \times Gradient	0.3316	0.7765	0.8655
Natural	LRP [Bach 2015]	0.1027	0.2487	0.7518
Natural	DeepLIFT [Shrikumar 2017]	0.2907	0.7641	0.8504
Natural	GradSHAP [Lundberg 2017]	0.2290	0.6513	0.8099
Natural	IG [Sundararajan 2017]	0.2638	0.7148	0.8380
PGD	Simple Gradient	0.1725	0.7245	0.8004
PGD	Image \times Gradient	0.1714	0.7269	0.8552
PGD	LRP [Bach 2015]	0.2374	0.4147	0.8161
PGD	DeepLIFT [Shrikumar 2017]	0.5572	0.9746	0.8977
PGD	GradSHAP [Lundberg 2017]	0.1714	0.7270	0.8552
PGD	IG [Sundararajan 2017]	0.1947	0.7335	0.8584

Table 2: Average top- k intersection, 3-LENS-prec@ k and 3-LENS-prec@ k -div for random sign perturbation attack applied to different attribution methods on ImageNet for naturally and adversarially(PGD)-trained ResNet50 models.

6 Conclusion and Future Work

We show that the fragility of attributions is an effect of using fragile robustness metrics such as top- k intersection that only look at the rank order of attributions and fail to capture the locality of pixel positions with high attributions. We highlight the need for locality-sensitive metrics for attributional robustness and propose natural locality-sensitive extensions of existing metrics. We introduce another method of picking diverse top- k pixels that can be naturally extended with locality to obtain improved measure of attributional robustness. Theoretical understanding of locality-sensitive metrics of attributional robustness, constructing stronger attributional attacks for these metrics, and using them to build attributionally robust models are important future directions.

References

- Adebayo, J.; Gilmer, J.; Muelly, M.; Goodfellow, I. J.; Hardt, M.; and Kim, B. 2018. Sanity Checks for Saliency Maps. In Bengio, S.; Wallach, H. M.; Larochelle, H.; Grauman, K.; Cesa-Bianchi, N.; and Garnett, R., eds., *Advances in Neural Information Processing Systems 31: Annual Conference on Neural Information Processing Systems 2018, NeurIPS 2018, December 3-8, 2018, Montréal, Canada*, 9525–9536.
- Agarwal, C.; Johnson, N.; Pawelczyk, M.; Krishna, S.; Saxena, E.; Zitnik, M.; and Lakkaraju, H. 2022. Rethinking Stability for Attribution-based Explanations. *arXiv preprint arXiv:2203.06877*.
- Alvarez-Melis, D.; and Jaakkola, T. S. 2018. On the robustness of interpretability methods. *arXiv preprint arXiv:1806.08049*.
- Arun, N.; Gaw, N.; Singh, P.; Chang, K.; Aggarwal, M.; Chen, B.; et al. 2020. Assessing the (Un) Trustworthiness of saliency maps for localizing abnormalities in medical imaging. *arXiv Preprint*].
- Bach, S.; Binder, A.; Montavon, G.; Klauschen, F.; Müller, K.-R.; and Samek, W. 2015. On Pixel-Wise Explanations for Non-Linear Classifier Decisions by Layer-Wise Relevance Propagation. In: *PloS One* 10.7 (2015), e0130140.
- Bhatt, U.; Weller, A.; and Moura, J. M. 2020. Evaluating and aggregating feature-based model explanations. *arXiv preprint arXiv:2005.00631*.
- Biggio, B.; Corona, I.; Maiorca, D.; Nelson, B.; Šrndić, N.; Laskov, P.; Giacinto, G.; and Roli, F. 2013. Evasion Attacks against Machine Learning at Test Time. *Lecture Notes in Computer Science*, 387–402.
- Boggust, A.; Suresh, H.; Strobel, H.; Gutttag, J. V.; and Satyanarayan, A. 2022. Beyond Faithfulness: A Framework to Characterize and Compare Saliency Methods. *CoRR*, abs/2206.02958.
- Carvalho, D. V.; Pereira, E. M.; and Cardoso, J. S. 2019. Machine learning interpretability: A survey on methods and metrics. *Electronics*, 8(8): 832.
- Chalasanani, P.; Chen, J.; Chowdhury, A. R.; Wu, X.; and Jha, S. 2020. Concise Explanations of Neural Networks using Adversarial Training. In *Proceedings of the 37th International Conference on Machine Learning, ICML 2020, 13-18 July 2020, Virtual Event*, volume 119 of *Proceedings of Machine Learning Research*, 1383–1391. PMLR.
- Chattopadhyay, A.; Sarkar, A.; Howlader, P.; and Balasubramanian, V. N. 2018. Grad-CAM++: Generalized Gradient-Based Visual Explanations for Deep Convolutional Networks. 839–847.
- Chen, J.; Wu, X.; Rastogi, V.; Liang, Y.; and Jha, S. 2019. Robust Attribution Regularization.
- Fagin, R.; Kumar, R.; and Sivakumar, D. 2003. Comparing Top k Lists. *SIAM Journal on Discrete Mathematics*, 17(1): 134–160.
- Fan, F.; Xiong, J.; Li, M.; and Wang, G. 2021. On Interpretability of Artificial Neural Networks: A Survey. *arXiv:2001.02522 [cs, stat]*.
- Fel, T.; Vigouroux, D.; Cadène, R.; and Serre, T. 2022. How good is your explanation? algorithmic stability measures to assess the quality of explanations for deep neural networks. In *Proceedings of the IEEE/CVF Winter Conference on Applications of Computer Vision*, 720–730.
- Gade, K.; Geyik, S. C.; Kenthapadi, K.; Mithal, V.; and Taly, A. 2020. Explainable AI in industry: practical challenges and lessons learned: implications tutorial. In Hildebrandt, M.; Castillo, C.; Celis, L. E.; Ruggieri, S.; Taylor, L.; and Zanfir-Fortuna, G., eds., *FAT* '20: Conference on Fairness, Accountability, and Transparency, Barcelona, Spain, January 27-30, 2020*, 699. ACM.
- Ghorbani, A.; Abid, A.; and Zou, J. Y. 2019. Interpretation of Neural Networks Is Fragile.
- Goodfellow, I. J.; Shlens, J.; and Szegedy, C. 2015. Explaining and Harnessing Adversarial Examples.
- He, K.; Zhang, X.; Ren, S.; and Sun, J. 2015. Deep Residual Learning for Image Recognition. *CoRR*, abs/1512.03385.
- Iandola, F. N.; Moskewicz, M. W.; Ashraf, K.; Han, S.; Dally, W. J.; and Keutzer, K. 2016. SqueezeNet: AlexNet-level accuracy with 50x fewer parameters and <1MB model size. *CoRR*, abs/1602.07360.
- Kim, B.; Wattenberg, M.; Gilmer, J.; Cai, C.; Wexler, J.; Viegas, F.; et al. 2018. Interpretability beyond feature attribution: Quantitative testing with concept activation vectors (tcav). In *International conference on machine learning*, 2668–2677. PMLR.
- Korte, B.; and Lovász, L. 1981. Mathematical structures underlying greedy algorithms. In Gécseg, F., ed., *Fundamentals of Computation Theory*, 205–209. Springer Berlin Heidelberg. ISBN 978-3-540-38765-7.
- Lakkaraju, H.; Arsov, N.; and Bastani, O. 2020. Robust and Stable Black Box Explanations. In *International Conference on Machine Learning*, 5628–5638.
- Lecue, F.; Guidotti, R.; Minervini, P.; and Giannotti, F. 2021. 2021 Explainable AI Tutorial. <https://xaitutorial2021.github.io/>. Visited on 14-09-2021.
- Lipton, Z. C. 2018. The mythos of model interpretability. *Commun. ACM*, 61(10): 36–43.
- Lundberg, S. M.; and Lee, S. 2017. A Unified Approach to Interpreting Model Predictions.
- Madry, A.; Makelov, A.; Schmidt, L.; Tsipras, D.; and Vladu, A. 2018. Towards Deep Learning Models Resistant to Adversarial Attacks.
- Molnar, C. 2019. *Interpretable Machine Learning*. <https://christophm.github.io/interpretable-ml-book/>.
- Nourelahi, M.; Kotthoff, L.; Chen, P.; and Nguyen, A. 2022. How explainable are adversarially-robust CNNs? *arXiv:2205.13042*.
- Oh, C.; and Jeong, J. 2020. VODCA: Verification of Diagnosis Using CAM-Based Approach for Explainable Process Monitoring. *Sensors*, 20(23): 6858.
- Oviedo, F.; Ferres, J. L.; Buonassisi, T.; and Butler, K. T. 2022. Interpretable and Explainable Machine Learning for Materials Science and Chemistry. *Accounts of Materials Research*, 3(6): 597–607.

- Ozdag, M. 2018. Adversarial Attacks and Defenses Against Deep Neural Networks: A Survey. *Procedia Computer Science*, 140: 152–161.
- Ribeiro, M. T.; Singh, S.; and Guestrin, C. 2016. "Why Should I Trust You?": Explaining the Predictions of Any Classifier.
- Samek, W.; Montavon, G.; Vedaldi, A.; Hansen, L. K.; and Müller, K., eds. 2019. *Explainable AI: Interpreting, Explaining and Visualizing Deep Learning*, volume 11700 of *Lecture Notes in Computer Science*. Springer. ISBN 978-3-030-28953-9.
- Sarkar, A.; Sarkar, A.; and Balasubramanian, V. N. 2021. Enhanced Regularizers for Attributional Robustness.
- Selvaraju, R. R.; Cogswell, M.; Das, A.; Vedantam, R.; Parikh, D.; and Batra, D. 2017. Grad-CAM: Visual Explanations from Deep Networks via Gradient-Based Localization. 618–626.
- Shrikumar, A.; Greenside, P.; and Kundaje, A. 2017. Learning Important Features Through Propagating Activation Differences.
- Shrikumar, A.; Greenside, P.; Shcherbina, A.; and Kundaje, A. 2016. Not Just a Black Box: Learning Important Features Through Propagating Activation Differences. 1605.01713.
- Silva, S. H.; and Najafirad, P. 2020. Opportunities and Challenges in Deep Learning Adversarial Robustness: A Survey. *CoRR*, abs/2007.00753.
- Simonyan, K.; Vedaldi, A.; and Zisserman, A. 2014. Deep Inside Convolutional Networks: Visualising Image Classification Models and Saliency Maps.
- Singh, M.; Kumari, N.; Mangla, P.; Sinha, A.; Balasubramanian, V. N.; and Krishnamurthy, B. 2020. Attributional Robustness Training Using Input-Gradient Spatial Alignment.
- Slack, D.; Hilgard, A.; Lakkaraju, H.; and Singh, S. 2021a. Counterfactual Explanations Can Be Manipulated. In *Advances in Neural Information Processing Systems*.
- Slack, D.; Hilgard, A.; Singh, S.; and Lakkaraju, H. 2021b. Reliable Post hoc Explanations: Modeling Uncertainty in Explainability. In *Advances in Neural Information Processing Systems*, 9391–9404.
- Slack, D.; Hilgard, S.; Jia, E.; Singh, S.; and Lakkaraju, H. 2020. Fooling LIME and SHAP: Adversarial Attacks on Post hoc Explanation Methods.
- Smilkov, D.; Thorat, N.; Kim, B.; Viégas, F. B.; and Wattenberg, M. 2017. SmoothGrad: removing noise by adding noise. 1706.03825.
- Springenberg, J. T.; Dosovitskiy, A.; Brox, T.; and Riedmiller, M. A. 2015. Striving for Simplicity: The All Convolutional Net.
- Sundararajan, M.; Taly, A.; and Yan, Q. 2017. Axiomatic Attribution for Deep Networks. In Precup, D.; and Teh, Y. W., eds., *Proceedings of the 34th International Conference on Machine Learning, ICML 2017, Sydney, NSW, Australia, 6-11 August 2017*, volume 70 of *Proceedings of Machine Learning Research*, 3319–3328. PMLR.
- Szegedy, C.; Zaremba, W.; Sutskever, I.; Bruna, J.; Erhan, D.; Goodfellow, I. J.; and Fergus, R. 2014. Intriguing properties of neural networks.
- Tang, S.; Ghorbani, A.; Yamashita, R.; Rehman, S.; Dunnmon, J. A.; Zou, J. Y.; and Rubin, D. L. 2021. Data Valuation for Medical Imaging Using Shapley Value: Application on A Large-scale Chest X-ray Dataset. *Scientific Reports(Nature Publisher Group)*.
- Tomsett, R.; Harborne, D.; Chakraborty, S.; Gurram, P.; and Preece, A. D. 2020. Sanity Checks for Saliency Metrics. In *The Thirty-Fourth AAAI Conference on Artificial Intelligence, AAAI 2020, The Thirty-Second Innovative Applications of Artificial Intelligence Conference, IAAI 2020, The Tenth AAAI Symposium on Educational Advances in Artificial Intelligence, EAAI 2020, New York, NY, USA, February 7-12, 2020*, 6021–6029. AAAI Press.
- Wang, F.; and Kong, A. W. 2022. Exploiting the Relationship Between Kendall’s Rank Correlation and Cosine Similarity for Attribution Protection. *CoRR*, abs/2205.07279.
- Wang, Z.; Wang, H.; Ramkumar, S.; Mardziel, P.; Fredrikson, M.; and Datta, A. 2020. Smoothed Geometry for Robust Attribution.
- Yap, M.; Johnston, R. L.; Foley, H.; MacDonald, S.; Kondrashova, O.; Tran, K. A.; Nones, K.; Koufariotis, L. T.; Bean, C.; Pearson, J. V.; Trzaskowski, M.; and Waddell, N. 2021. Verifying explainability of a deep learning tissue classifier trained on RNA-seq data. *Scientific Reports(Nature Publisher Group)*.
- Yeh, C.-K.; Hsieh, C.-Y.; Suggala, A.; Inouye, D. I.; and Ravikumar, P. K. 2019. On the (in) fidelity and sensitivity of explanations. *Advances in Neural Information Processing Systems*, 32.
- Zeiler, M. D.; and Fergus, R. 2014. Visualizing and Understanding Convolutional Networks. In *Proceedings of The European Conference on Computer Vision (ECCV)*.
- Zeiler, M. D.; Krishnan, D.; Taylor, G. W.; and Fergus, R. 2010. Deconvolutional networks. In *The Twenty-Third IEEE Conference on Computer Vision and Pattern Recognition, CVPR 2010, San Francisco, CA, USA, 13-18 June 2010*, 2528–2535. IEEE Computer Society.
- Zhang, Y.; Tiño, P.; Leonardis, A.; and Tang, K. 2020. A Survey on Neural Network Interpretability. *arXiv:2012.14261 [cs]*.
- Zhou, B.; Khosla, A.; Lapedriza, À.; Oliva, A.; and Torralba, A. 2016. Learning Deep Features for Discriminative Localization. In *2016 IEEE Conference on Computer Vision and Pattern Recognition, CVPR 2016, Las Vegas, NV, USA, June 27-30, 2016*, 2921–2929. IEEE Computer Society.

A Supplementary : Rethinking Robustness of Model Attributions

The Appendix contains proofs, additional experiments to show that the trends hold across different datasets and other ablation studies which could not be included in the main paper due to space constraints.

B Attributional Robustness Metrics are Weak

In this section, we empirically show that the existing metrics for attributional robustness are weak and inadequate as they allow even a small random perturbation to appear like a decent attributional attack.

B.1 Random Vectors are Attributional Attacks under Existing Metrics

Random vectors of a small ℓ_∞ norm are often used as baselines of input perturbations (both in adversarial robustness (Silva and Najafirad 2020) and attributional robustness literature (Ghorbani, Abid, and Zou 2019)), since it is known that predictions of neural network models are known to be resilient to random perturbations of inputs. Previous work by Ghorbani, Abid, and Zou (2019) has shown random perturbations to be a reasonable baseline to compare against their attributional attack. Extending it further, we show that a single input-agnostic random perturbation happens to be an effective *universal* attributional attack if we measure attributional robustness using a weak metric based on top- k intersection. In other words, considering even a random perturbation happens to be a good attributional attack under such metrics, we show that existing metrics for attributional robustness such as top- k intersection are extremely fragile, i.e., they would unfairly deem many attribution methods as fragile.

Integrated Gradients (IG) is a well-known attribution method based on well-defined axiomatic foundations (Sundararajan, Taly, and Yan 2017), which is commonly used in attributional robustness literature (Chen et al. 2019; Sarkar, Sarkar, and Balasubramanian 2021). We take a naturally trained CNN model on MNIST and perturb the images using a random perturbation (an independent random perturbation per input image) as well as a single, input-agnostic or *universal* random perturbation for all images. Figure 9 shows a sample image from the MNIST dataset and the visual difference between the IG of the original image, the IG after adding a random perturbation, and the IG after adding a *universal* random perturbation. The IG after the universal random attack (Figure 9d) is visually more dissimilar to the IG of the original image (Figure 9b) than the IG of a simple random perturbation (Figure 9c). (Note that top- k intersection between Figure 9b and 9c is only 0.62, although the two look similar. As stated in the caption, a locality-sensitive metric shows them to be closer in attribution however.)

Similarly, Table 3 shows that under existing metrics to quantify attributional robustness of IG on a naturally trained CNN model, even a single, input-agnostic or *universal* random perturbation can sometimes be a more effective attribu-

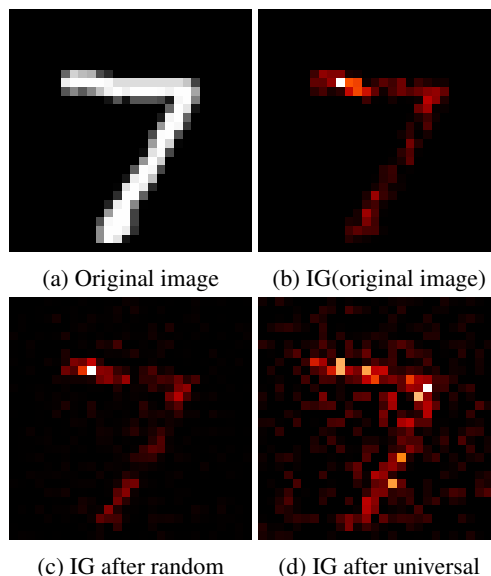


Figure 9: Sample image from MNIST on LeNet based model shows that the Integrated Gradients (IG) after a universal random perturbation are more dissimilar than IG after a simple, independent random perturbation for each input. All perturbations have random ± 1 coordinates, scaled down to have ℓ_∞ norm $\epsilon = 0.3$. (c) has a top- k intersection of 0.68, while (d) has a top- k intersection of 0.62. With our locality-sensitive metric, (c) has 1-LENS@ k of 0.99 and (d) has 1-LENS@ k of 1.0.

tional attack than using an independent random perturbation for each input.

Dataset	Perturbation	top- k intersection	Spearman's ρ	Kendall's τ
MNIST	random	0.7500	0.5347	0.4337
	universal random	0.5855	0.4831	0.4063
Fashion MNIST	random	0.5385	0.6791	0.5152
	universal random	0.5280	0.7154	0.5688
GTSRB	random	0.8216	0.9433	0.8136
	universal random	0.9293	0.9887	0.9243
Flower	random	0.8202	0.9562	0.8340
	universal random	0.9344	0.9908	0.9321

Table 3: Attributional robustness of IG on naturally trained models measured using average top- k intersection, Spearman's ρ and Kendall's τ between IG(original image) and IG(perturbed image). $k = 100$ for MNIST, Fashion MNIST, GTSRB and $k = 1000$ for Flower.

C Details of Experimental Setup

The detailed description of the setup used in our experiments.

Datasets: We use the standard benchmark train-test split of all the datasets used in this work, that is publicly available. MNIST dataset consists of 70,000 images of 28×28 size, divided into 10 classes: 60,000 used for training and 10,000 for testing. Fashion MNIST dataset consists of 70,000 images of 28×28 size, divided into 10 classes: 60,000 used for training and 10,000 for testing. GTSRB dataset con-

sists of 51,739 images of 32×32 size, divided into 43 classes: 34,699 used for training, 4,410 for validation and 12,630 for testing. Flower dataset consist of 1,360 images of 128×128 size, divided into 17 classes: 1,224 used for training and 136 for testing. GTSRB and Flower datasets were preprocessed exactly as given in (Chen et al. 2019)[Appendix C] for consistency of results. ImageNet dataset consists of images of 227×227 size, divided into 1000 classes. 50,000 for validation were used to obtain samples for testing.

Architectures: For MNIST, Fashion MNIST, GTSRB and Flower datasets we use the exact architectures as used by Chen et al. (2019), ImageNet dataset we use SqueezeNet(Iandola et al. 2016) as given by Ghorbani, Abid, and Zou (2019) and ResNet50(He et al. 2015).

Attribution robustness metrics: We use the same comparison metrics as used by Ghorbani, Abid, and Zou (2019) and Chen et al. (2019) like top- k pixels intersection, Spearman’s ρ and Kendall’s τ rank correlation to compare attribution maps of the original and perturbed images. The k value for top- k attack along with settings like step size, number of steps and number of times attack is to be applied is as used by Chen et al. (2019) for the attack construction : MNIST(200,0.01,100,3), Fashion MNIST(100,0.01,100,3), GTSRB(100,1.0,50,3), Flower(1000,1.0,100,3) and ImageNet(1000,1.0,100,3) (Ghorbani, Abid, and Zou 2019).

Sample sizes for attribution robustness evaluations: IG based experiments For MNIST, Fashion MNIST and Flower with fixed top- k attack similar to Chen et al. (2019) the complete test set were used to obtain the results. For GTSRB a random sample of size 1000 was used for all the experiments. *Simple gradient based experiments* For MNIST and Fashion MNIST a random sample of 2500/1000 from the test set. For GTSRB, a random sample of size 1000 and the complete test set for the Flower dataset. For ImageNet, we used the samples provide by Ghorbani, Abid, and Zou (2019). We used around 500 random samples for the random sign perturbation results using Pytorch/Captum.

Adversarial training: We use the standard setup as used by (Chen et al. 2019). We perform PGD based adversarial training with the provided ϵ budget using the following settings (number of steps, step size) for PGD : MNIST (40,0.01), Fashion MNIST(20,0.01), GTSRB(7,2/255), Flower(7,2/255). For ImageNet, we used the PGD based pre-trained ResNet50 model with ℓ_∞ -norm of $\epsilon = 8/255$ provided in the robustness package².

Training for Attributional Robustness: We use the IG-SUM-NORM objective function for all the datasets study based on (Chen et al. 2019) based training. With the exact setting as given in paper with code³.

Hardware Configuration: We used a server with 4 Nvidia GeForce GTX 1080i GPU and a server with 8 Nvidia Tesla V100 GPU to run the experiments in the paper.

Explanation methods: The Tensorflow⁴ code for IG, SG, DeepLIFT we used (Chen et al. 2019) and Ghorbani, Abid,

and Zou (2019) depending on the dataset. We used Pytorch⁵-Captum⁶ to obtain the various explanation maps with the random sign perturbation experiments.

D Proofs from Section 3.1

We restate and prove Proposition 1 below.

Proposition 4. For any $w_1 \leq w_2$, we have $d_k^{(w_2)}(\mathbf{a}_1, \mathbf{a}_2) \leq d_k^{(w_1)}(\mathbf{a}_1, \mathbf{a}_2) \leq |S_k \Delta T_k|/k$, where Δ denotes the symmetric set difference, i.e., $A \Delta B = (A \setminus B) \cup (B \setminus A)$.

Proof. The inequalities follows immediately using $S \subseteq N_{w_1}(S) \subseteq N_{w_2}(S)$, for any S , and hence, $|S \setminus N_w(T)| \leq |S \setminus T|$, for any S, T and w . \square

We restate and prove Proposition 2 below.

Proposition 5. $d(\mathbf{a}_1, \mathbf{a}_2)$ defined above is upper bounded by $u(\mathbf{a}_1, \mathbf{a}_2)$ given by

$$u(\mathbf{a}_1, \mathbf{a}_2) = \sum_{k=1}^{\infty} \alpha_k \sum_{w=0}^{\infty} \beta_w \frac{|S_k \Delta T_k|}{k},$$

and $u(\mathbf{a}_1, \mathbf{a}_2)$ defines a bounded metric on the space of attribution vectors.

Proof. Proof follows from Proposition 1 and using the fact that symmetric set difference satisfies triangle inequality. \square

We restate and prove Proposition 3 below.

Proposition 6. For any inputs x, y and any $w \geq 0$, $\|\tilde{\mathbf{a}}^{(w)}(x) - \tilde{\mathbf{a}}^{(w)}(y)\|_2 \leq \|\mathbf{a}(x) - \mathbf{a}(y)\|_2$.

Proof. $\|\tilde{\mathbf{a}}^{(w)}(x) - \tilde{\mathbf{a}}^{(w)}(y)\|_2^2$

$$= \sum_{1 \leq i, j \leq n} \left(\tilde{a}_{ij}^{(w)}(x) - \tilde{a}_{ij}^{(w)}(y) \right)^2$$

$$= \sum_{1 \leq i, j \leq n} \frac{1}{(2w+1)^4} \left(\sum_{\substack{(p,q) \in N_w(i,j), \\ 1 \leq p, q \leq n}} (a_{pq}(x) - a_{pq}(y)) \right)^2$$

$$\leq \sum_{1 \leq i, j \leq n} \frac{(2w+1)^2}{(2w+1)^4} \sum_{\substack{(p,q) \in N_w(i,j), \\ 1 \leq p, q \leq n}} (a_{pq}(x) - a_{pq}(y))^2$$

by Cauchy-Schwarz inequality

$$= \frac{1}{(2w+1)^2} \sum_{1 \leq i, j \leq n} \sum_{\substack{(p,q) \in N_w(i,j), \\ 1 \leq p, q \leq n}} (a_{pq}(x) - a_{pq}(y))^2$$

$$\leq \frac{(2w+1)^2}{(2w+1)^2} \sum_{1 \leq p, q \leq n} (a_{pq}(x) - a_{pq}(y))^2$$

²<https://github.com/MadryLab/robustness/>

³<https://github.com/jfc43/robust-attribution-regularization>

⁴<https://www.tensorflow.org>

⁵<https://github.com/pytorch>

⁶<https://github.com/pytorch/captum>

because each (p, q) appears in at most $(2w+1)^2$ possible $N_w(i, j)$'s

$$= \|\mathbf{a}(x) - \mathbf{a}(y)\|_2^2.$$

□

E Additional results for Section 3

E.1 Additional results for Section 3.2

The effect of varying k . Figure 10 shows a large disparity between top- k intersection and 1-LENS-prec@ k even when k is large. Figure 10 shows that top- k intersection can be very low even when the IG of the original and the IG of the perturbed images are locally very similar, as indicated by high 1-LENS-prec@ k . Our observation holds for the perturbations obtained by the top- k attack (Ghorbani, Abid, and Zou 2019) as well as a random perturbation across all datasets in our experiments. Figure 11 and 12 show the results on PGD and IG-SUM-NORM trained networks.

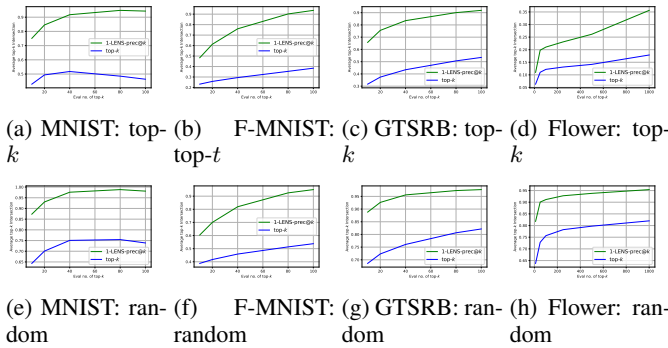


Figure 10: Attributional robustness of IG on naturally trained models measured as average top- k intersection and 1-LENS-prec@ k between IG(original image) and IG(perturbed image). Perturbations are obtained by the **top- k attack** (Ghorbani, Abid, and Zou 2019) and random perturbation. The plots show how the above measures change with varying k across different datasets.

Comparison of Spearman’s ρ and Kendall’s τ with 1-LENS-Spearman and 1-LENS-Kendall.

Figure 13 compares Spearman’s ρ and Kendall’s τ with 1-LENS-Spearman and 1-LENS-Kendall measures for attributional robustness. We observe that 1-smoothing of attribution maps increases the corresponding Kendall’s τ and Spearman’s ρ measures of attributional robustness, and this observation holds across all datasets in our experiments. As a result, we believe that 1-LENS-Spearman and 1-LENS-Kendall result in better or tighter attributional robustness measures than Spearman’s ρ and Kendall’s τ . Additional results in Figure 14.

Modifying the attack of Ghorbani, Abid, and Zou (2019) for 1-LENS-prec@ k objective A natural question is whether the original top- k attack of Ghorbani, Abid, and

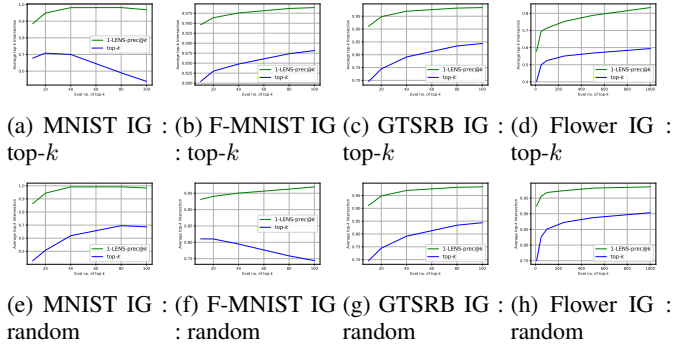


Figure 11: Attributional robustness of IG on adversarially (PGD) trained models measured as average top- k intersection and 1-LENS-prec@ k between IG(original image) and IG(perturbed image). Perturbations are obtained by the **top- k attack** (Ghorbani, Abid, and Zou 2019) and random perturbation. The plots show how the above measures change with varying k across different datasets.

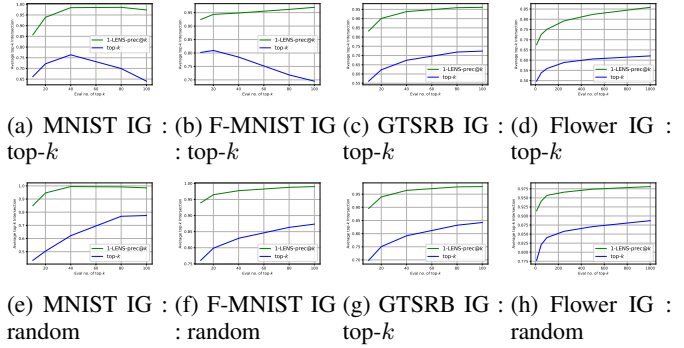


Figure 12: Attributional robustness of IG on IG-SUM-NORM trained models measured as average top- k intersection and 1-LENS-prec@ k between IG(original image) and IG(perturbed image). Perturbations are obtained by the **top- k attack** (Ghorbani, Abid, and Zou 2019) and random perturbation. The plots show how the above measures change with varying k across different datasets.

Zou (2019) seem weaker under locality-sensitive robustness measures only because the attack was specifically constructed for a corresponding top- k intersection objective. Since the construction of the attack in Ghorbani, Abid, and Zou (2019) is modifiable for any similarity objective, we use 1-LENS-prec@ k to construct a new attributional attack for 1-LENS-prec@ k objective based on the $k \times k$ neighborhood of pixels. Surprisingly, we notice that it leads to a *worse* attributional attack, if we measure its effectiveness using the top- k intersection; see Figure 15. In other words, attributional attacks against locality-sensitive measures of attributional robustness are non-trivial and may require fundamentally different ideas.

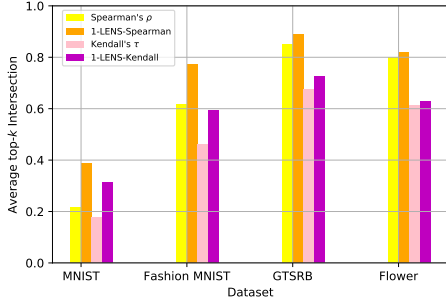


Figure 13: Attributional robustness of IG on naturally trained models measured as average Spearman’s ρ , 1-LENS-Spearman, Kendall τ and 1-LENS-Kendall between IG(original image) and IG(perturbed image). The perturbations are obtained by the top- t attack of Ghorbani, Abid, and Zou (2019).

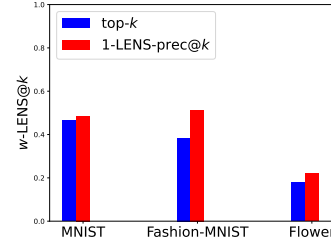


Figure 15: Average top- k intersection between IG(original image) and IG(perturbed image) on naturally trained models where the perturbation is obtained by incorporating 1-LENS-prec@ k objective in the Ghorbani, Abid, and Zou (2019) attack.

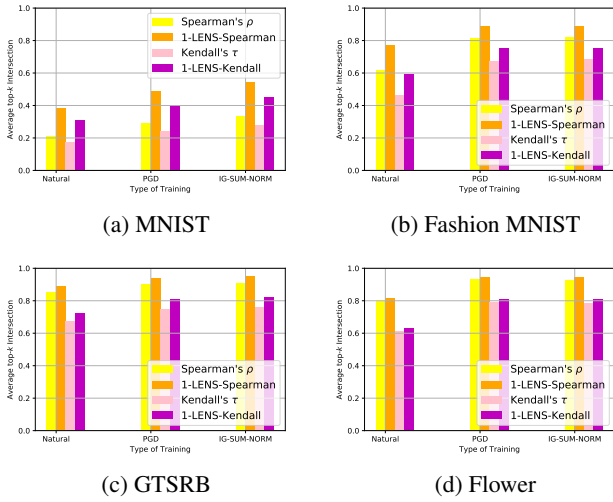


Figure 14: Average Kendall’s τ , Spearman’s ρ , 1-LENS-Kendall and 1-LENS-Spearman used to measure the attributional robustness of IG on naturally trained, PGD-trained and IG-SUM-NORM trained models. The perturbation used is the **top- k attack** of Ghorbani, Abid, and Zou (2019). Shown for (a) MNIST, (b) Fashion MNIST, (c) GTSRB and (d) Flower datasets.

E.2 Experiments with Integrated Gradients

Below we present additional experimental results for Integrated Gradients (IG).

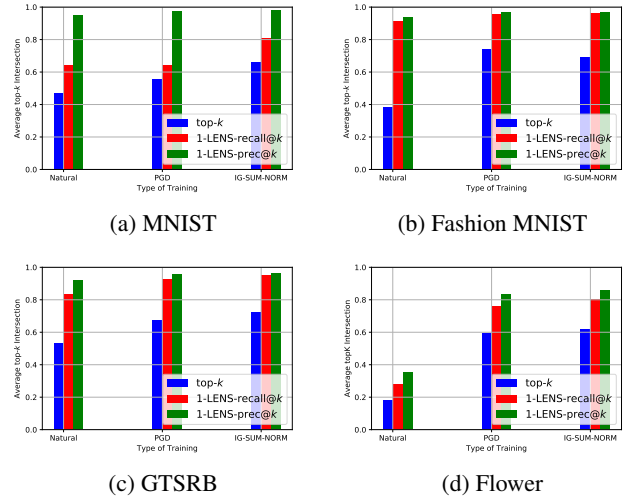


Figure 16: Average top- k intersection, 1-LENS-prec@ k , 1-LENS-recall@ k measured between IG(original image) and IG(perturbed image) for models that are naturally trained, PGD-trained and IG-SUM-NORM trained. The perturbation used is the **top- k attack** of (Ghorbani, Abid, and Zou 2019). Shown for (a) MNIST, (b) Fashion MNIST, (c) GTSRB and (d) Flower datasets.

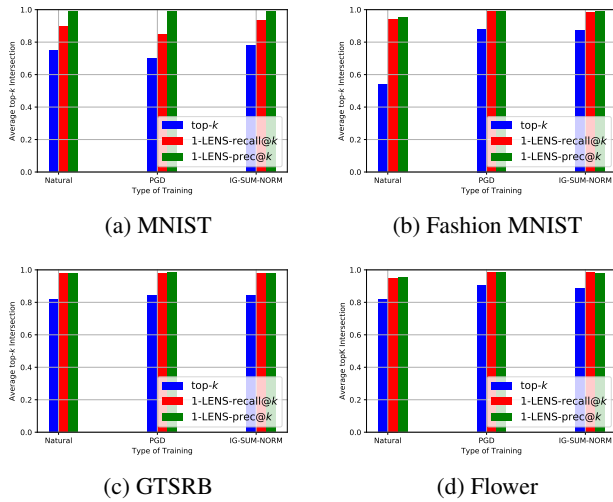


Figure 17: Attributional robustness of IG on naturally, PGD and IG-SUM-NORM trained models measured as top- k intersection, 1-LENS-prec@ k and 1-LENS-recall@ k between the IG of the original images and the IG of their perturbations obtained by the **random sign** attack (Ghorbani, Abid, and Zou 2019) across different datasets.

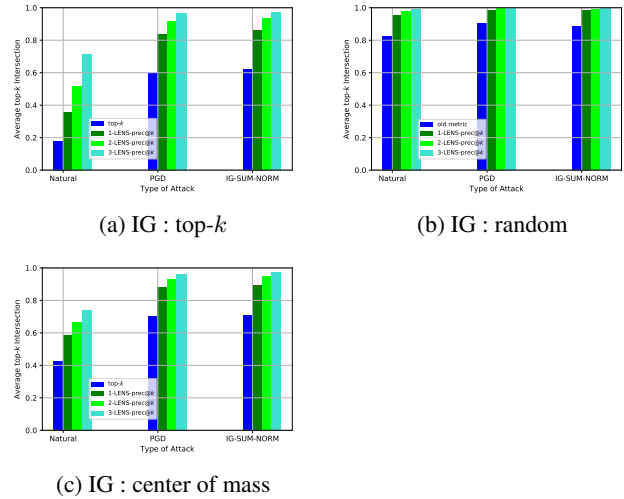


Figure 19: Attributional robustness of IG on naturally, PGD and IG-SUM-NORM trained models measured as top- k intersection and w -LENS-prec@ k between the IG of the original images and the IG of their perturbations. Perturbations are obtained by the top- k attack and the mass center attack (Ghorbani, Abid, and Zou 2019) as well as a random perturbation. The plots show the effect of varying w on Flower dataset.

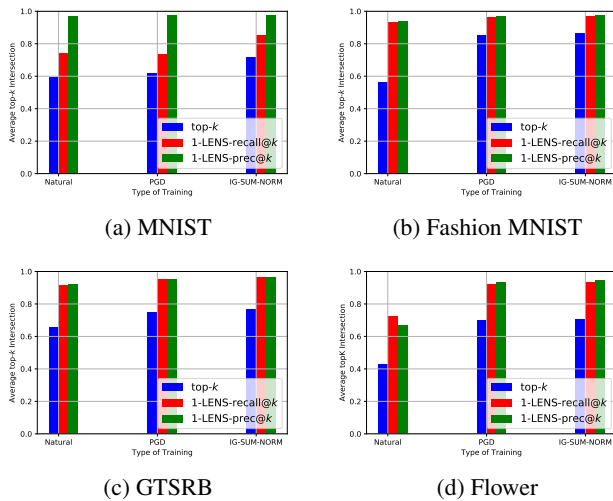


Figure 18: Attributional robustness of IG on naturally, PGD and IG-SUM-NORM trained models measured as top- k intersection, 1-LENS-prec@ k and 1-LENS-recall@ k between the IG of the original images and the IG of their perturbations obtained by the **mass center** attack (Ghorbani, Abid, and Zou 2019) across different datasets.

E.3 Experiments with Simple Gradients

We observe that our conclusions about Integrated Gradients (IG) continue to hold qualitatively, even if we replace IG with Simple Gradients as our attribution method.

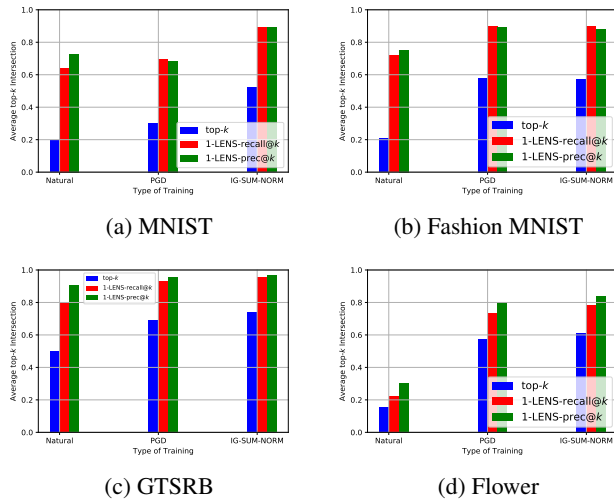


Figure 20: Attributional robustness of Simple Gradients on naturally, PGD and IG-SUM-NORM trained models measured as top- k intersection, 1-LENS-prec@ k and 1-LENS-recall@ k between the Simple Gradient of the original images and the Simple Gradient of their perturbations obtained by the **top- k** attack (Ghorbani, Abid, and Zou 2019) across different datasets.

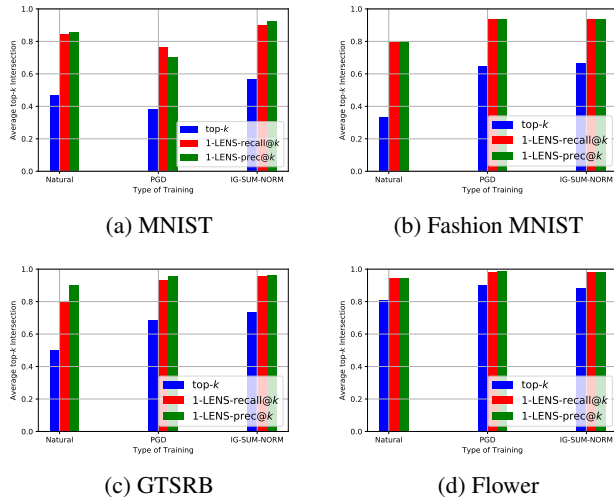


Figure 21: Attributional robustness of Simple Gradients on naturally, PGD and IG-SUM-NORM trained models measured as top- k intersection, 1-LENS-prec@ k and 1-LENS-recall@ k between the Simple Gradient of the original images and the Simple Gradient of their perturbations obtained by the **random sign** attack (Ghorbani, Abid, and Zou 2019) across different datasets.

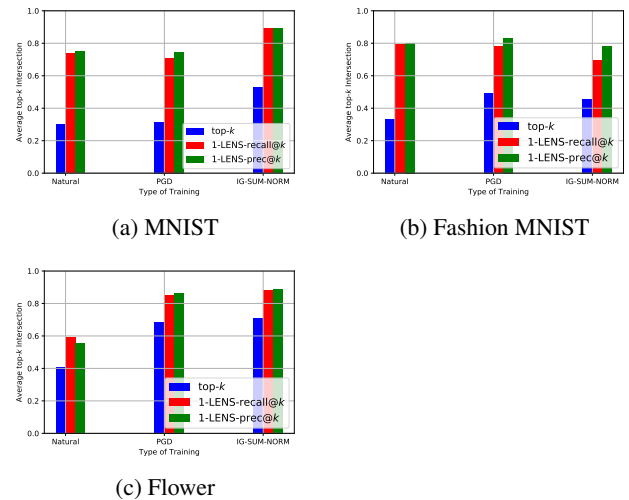


Figure 22: Attributional robustness of Simple Gradients on naturally, PGD and IG-SUM-NORM trained models measured as top- k intersection, 1-LENS-prec@ k and 1-LENS-recall@ k between the Simple Gradient of the original images and the Simple Gradient of their perturbations obtained by the **mass center** attack (Ghorbani, Abid, and Zou 2019) across different datasets.

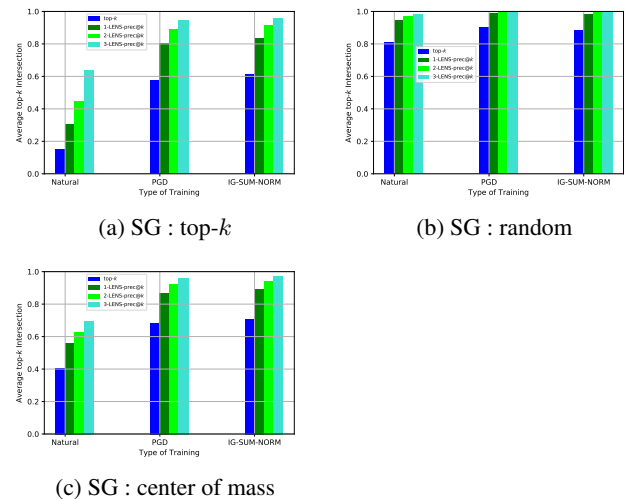


Figure 23: Attributional robustness of Simple Gradients on naturally, PGD and IG-SUM-NORM trained models measured as top- k intersection and w -LENS-prec@ k between the IG of the original images and the IG of their perturbations. Perturbations are obtained by the top- k attack and the mass center attack (Ghorbani, Abid, and Zou 2019) as well as a random perturbation. The plots show the effect of varying w on Flower dataset.

E.4 Experiments with Other Explanation Methods

In this section we present all the results with other explanation methods other than IG and SG shown in previous sections with naturally and PGD trained models using mainly random sign perturbation.

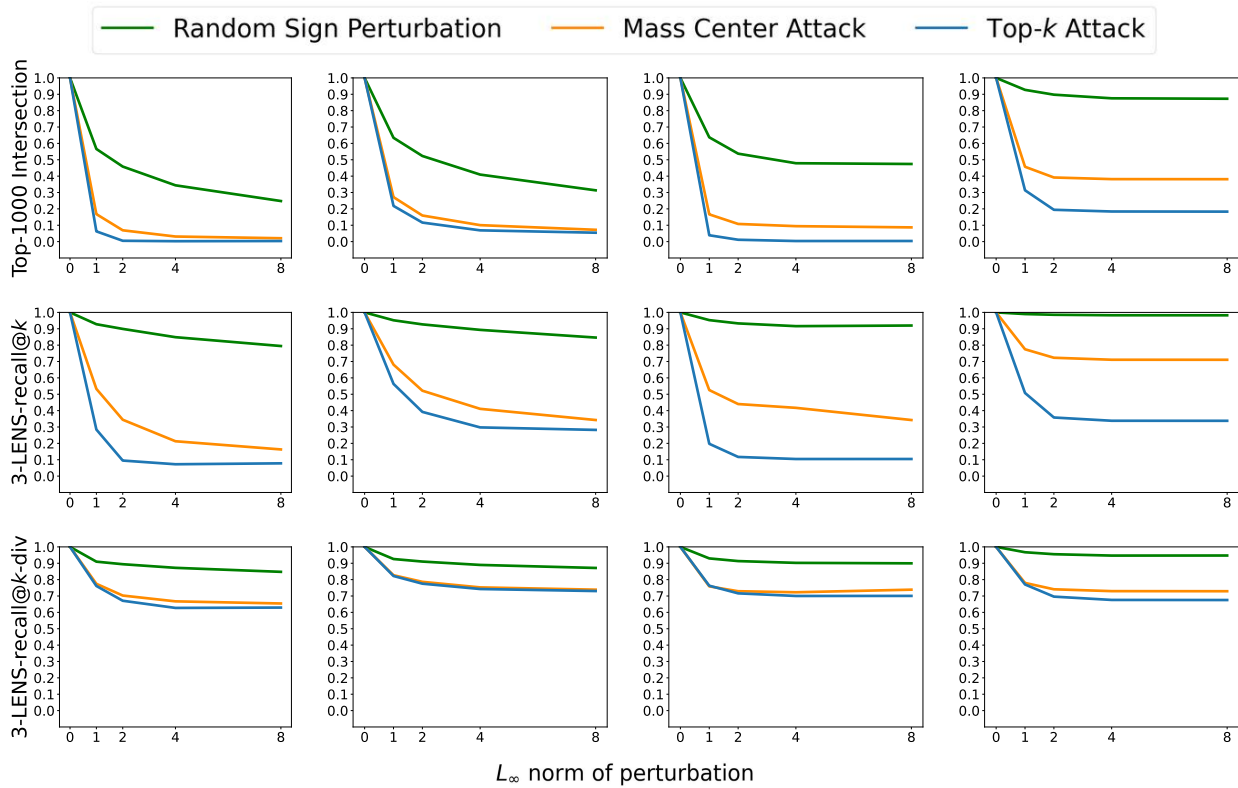


Figure 24: Similar to Figure 2, From top to bottom, we plot average top- k intersection (currently used metric, *top*), 3-LENS-recall@ k and 3-LENS-recall@ k -div (proposed metrics, *middle* and *bottom* respectively) against attributional attack perturbations for four attribution methods of a SqueezeNet model (as used by Ghorbani, Abid, and Zou (2019)) on Imagenet: (*left*) Simple Gradients (SG), (*center left*) Integrated Gradients (IG), (*center right*) DeepLift, (*right*) Deep Taylor Decomposition. We use $k = 1000$ with an ℓ_∞ -norm attack and three attack variants proposed by Ghorbani, Abid, and Zou (2019). Evidently, the proposed metrics show more robustness under the same attacks.

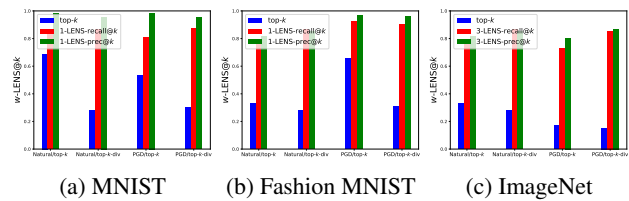
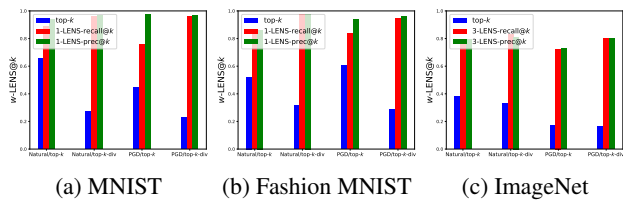


Figure 25: Attributional robustness of Simple Gradients(SG) on naturally and PGD trained models measured as top- k intersection, w -LENS-prec@ k and w -LENS-recall@ k between the **Simple Gradients(SG)** of the original images and of their perturbations obtained by the random sign perturbation across different datasets.

Figure 26: Attributional robustness of Image \times Gradients on naturally and PGD trained models measured as top- k intersection, w -LENS-prec@ k and w -LENS-recall@ k between the **Image \times Gradients** of the original images and of their perturbations obtained by the random sign perturbation across different datasets.

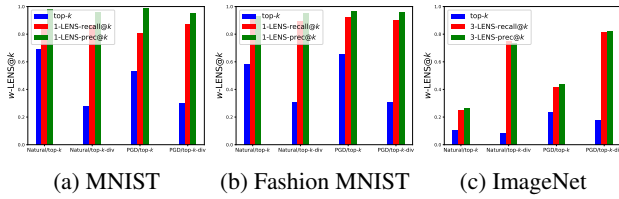


Figure 27: Attributional robustness of LRP (Bach et al. 2015) on naturally and PGD trained models measured as top- k intersection, w -LENS-prec@ k and w -LENS-recall@ k between the **LRP** of the original images and of their perturbations obtained by the random sign perturbation across different datasets.

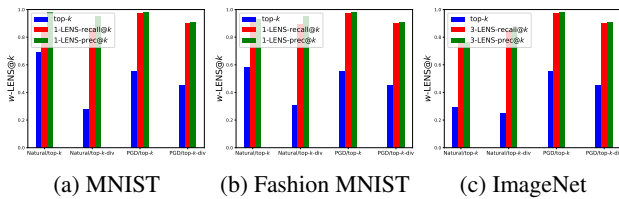


Figure 28: Attributional robustness of DeepLIFT (Shrikumar, Greenside, and Kundaje 2017) on naturally and PGD trained models measured as top- w intersection, w -LENS-prec@ k and w -LENS-recall@ k between the **DeepLIFT** of the original images and of their perturbations obtained by the random sign perturbation across different datasets.

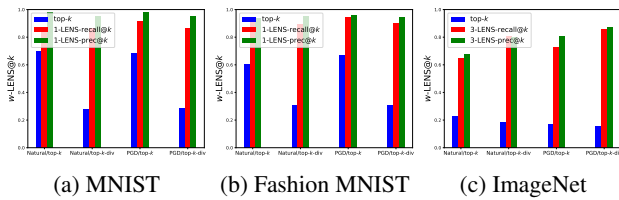


Figure 29: Attributional robustness of GradSHAP (Lundberg and Lee 2017) on naturally and PGD trained models measured as top- k intersection, w -LENS-prec@ k and w -LENS-recall@ k between the **GradSHAP** of the original images and of their perturbations obtained by the random sign perturbation across different datasets.

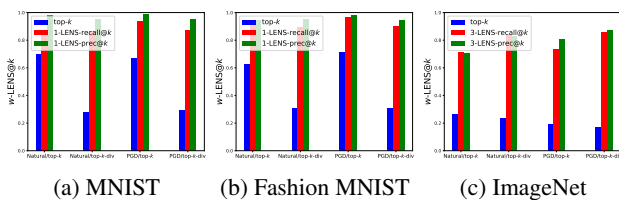


Figure 30: Attributional robustness of Integrated Gradients (Sundararajan, Taly, and Yan 2017) on naturally and PGD trained models measured as top- k intersection, w -LENS-prec@ k and w -LENS-recall@ k between the **Integrated Gradients** of the original images and of their perturbations obtained by the random sign perturbation across different datasets.

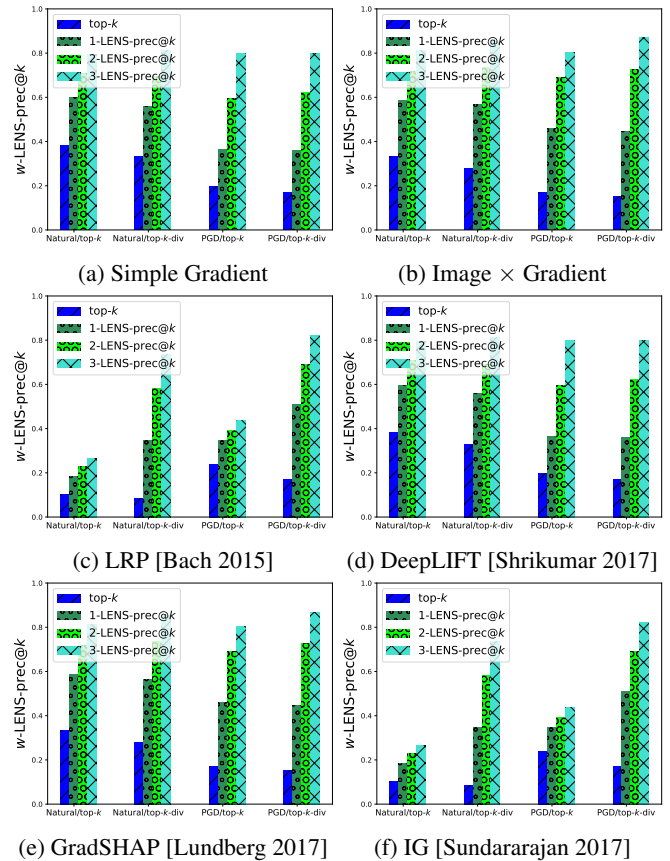


Figure 31: Attributional robustness of explanation methods on naturally and PGD trained models measured as top- k intersection and w -LENS-prec@ k between the explanation map of the original images and their perturbations. Perturbations are obtained by the random sign perturbation. The plots show the effect of varying w on ImageNet dataset with naturally and PGD trained ResNet50 model.

F The fragility of top- k intersection

Figure 32 highlights the top-100 pixels in the unperturbed and perturbed maps of a sample image. Figure 33, 34 show the top-1000 pixels and top-1000 diverse pixels along with w -LENS-recall@ k and w -LENS-prec@ k on them. Figure 35 visualize the top-1000 diverse pixels obtained with different window sizes eg. 3 and 5, respectively. Figure 36 elaborates the use of LENS(locality) and Figure 37 shows LENS-div(diversity) for the same example from ImageNet. Zoom in required to observe the finer details.

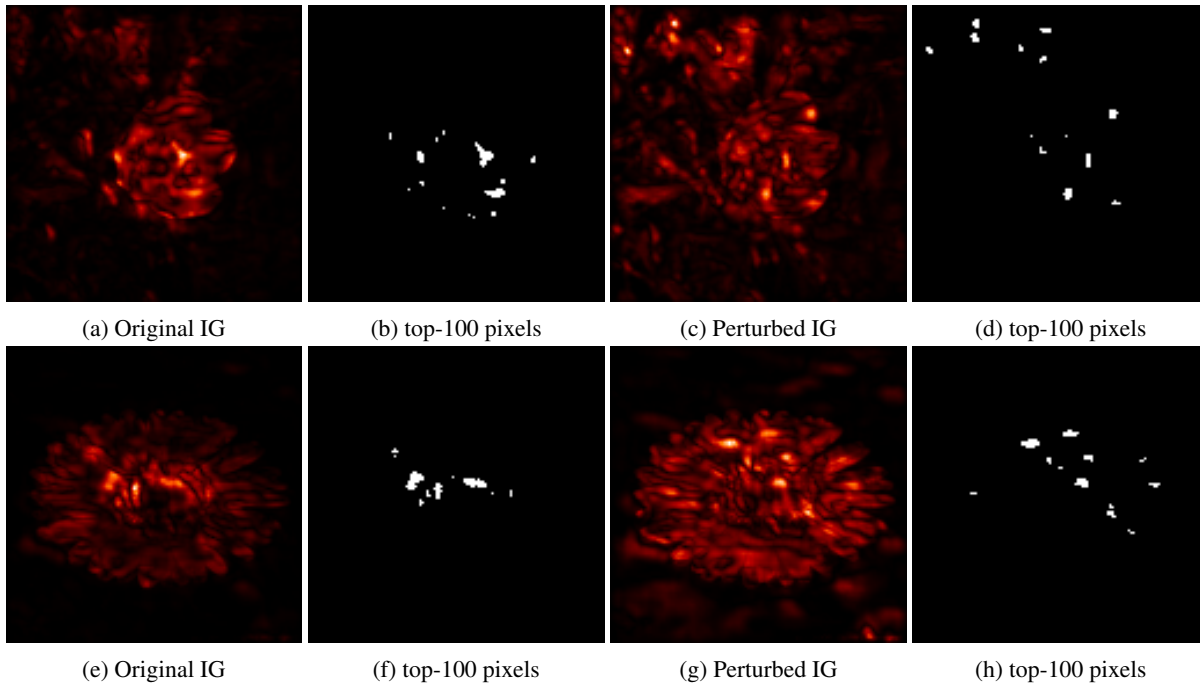


Figure 32: Sample Integrated Gradients(IG) map using Flower dataset where top-100 is highlighted before and after image is perturbed with top- k attack of Ghorbani, Abid, and Zou (2019).

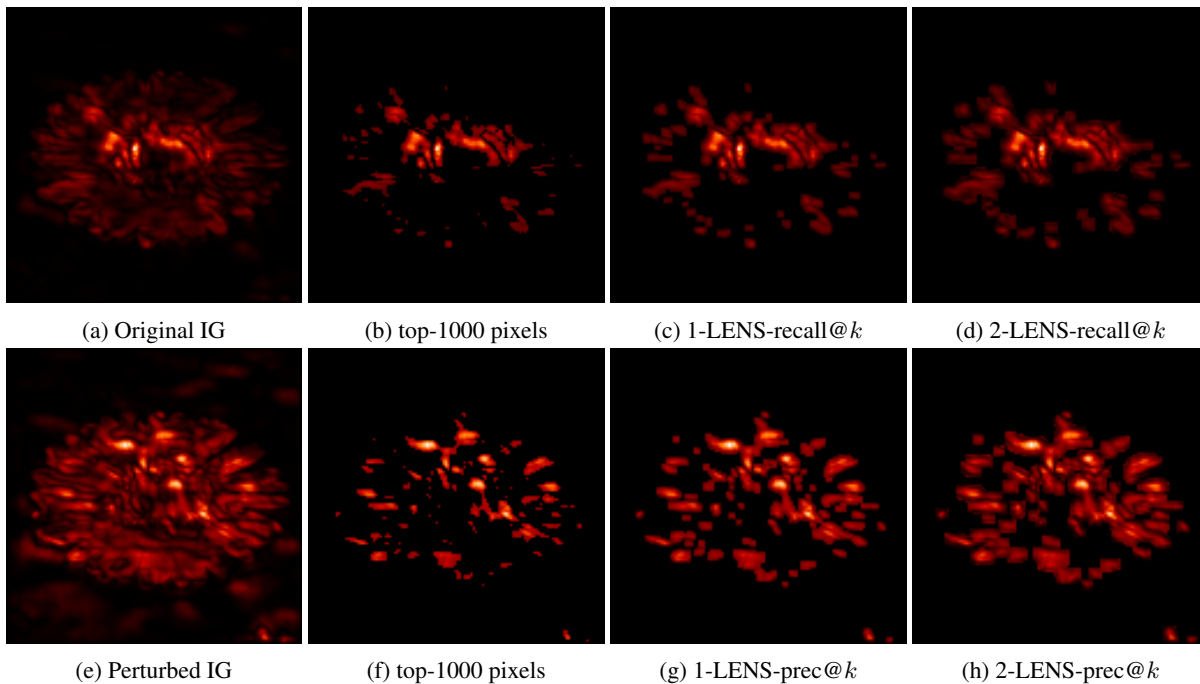


Figure 33: Example based on locality. Sample Integrated Gradients(IG) map using Flower dataset with top- k highlighted followed by w -LENS@ k maps (row 1) Original IG and (row 2) Perturbed IG with top- k attack (Ghorbani, Abid, and Zou 2019).

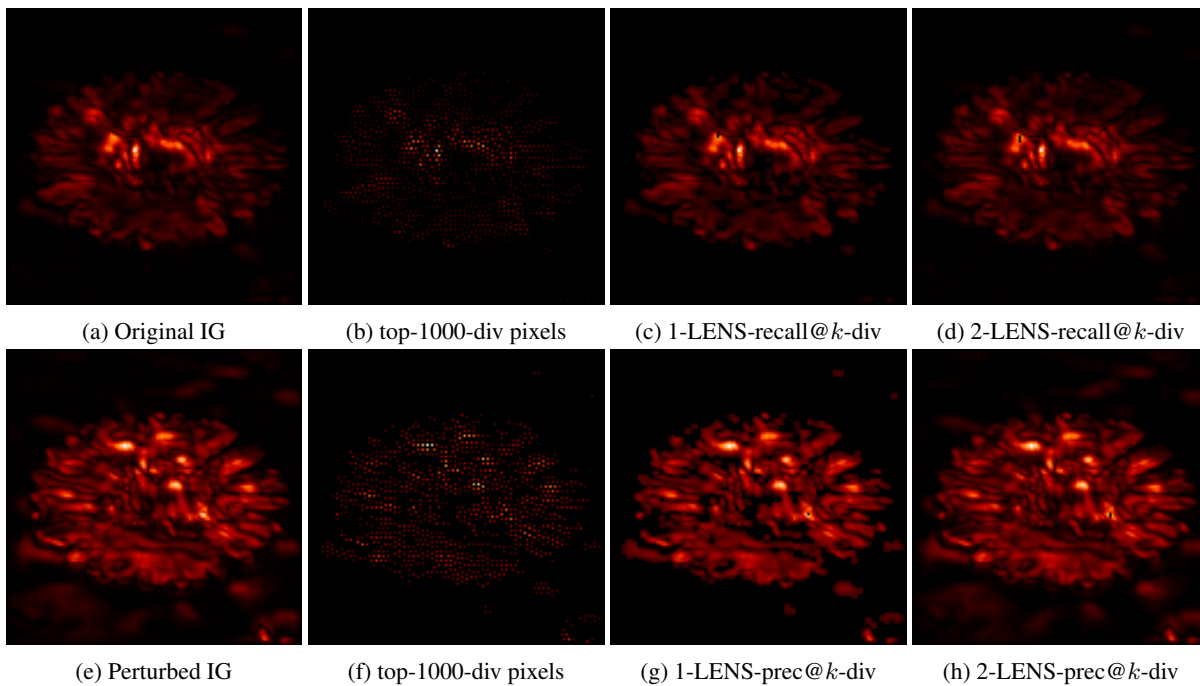


Figure 34: Example based on diversity. Sample Integrated Gradients(IG) map using Flower dataset with top- k -div highlighted followed by w -LENS@ k -div maps (row 1) Original IG and (row 2) Perturbed IG with top- k attack (Ghorbani, Abid, and Zou 2019).

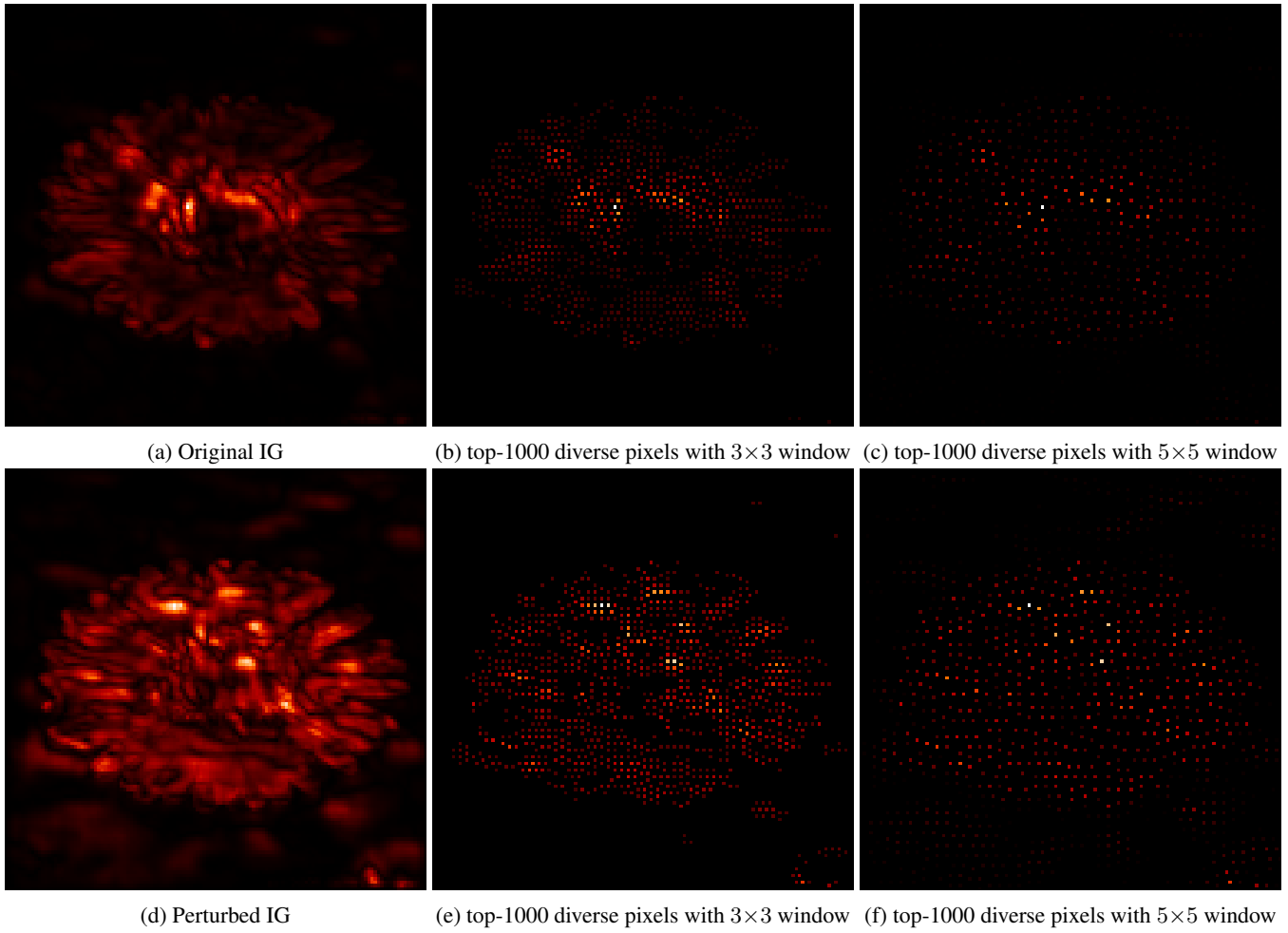


Figure 35: Example based on diversity with different window sizes. Sample Integrated Gradients(IG) map using Flower dataset with top- k -div highlighted with (column 2) 3×3 window (column 3) 5×5 window. (column 1) (top) map of unperturbed image (bottom) map of perturbed image with top- k attack (Ghorbani, Abid, and Zou 2019).

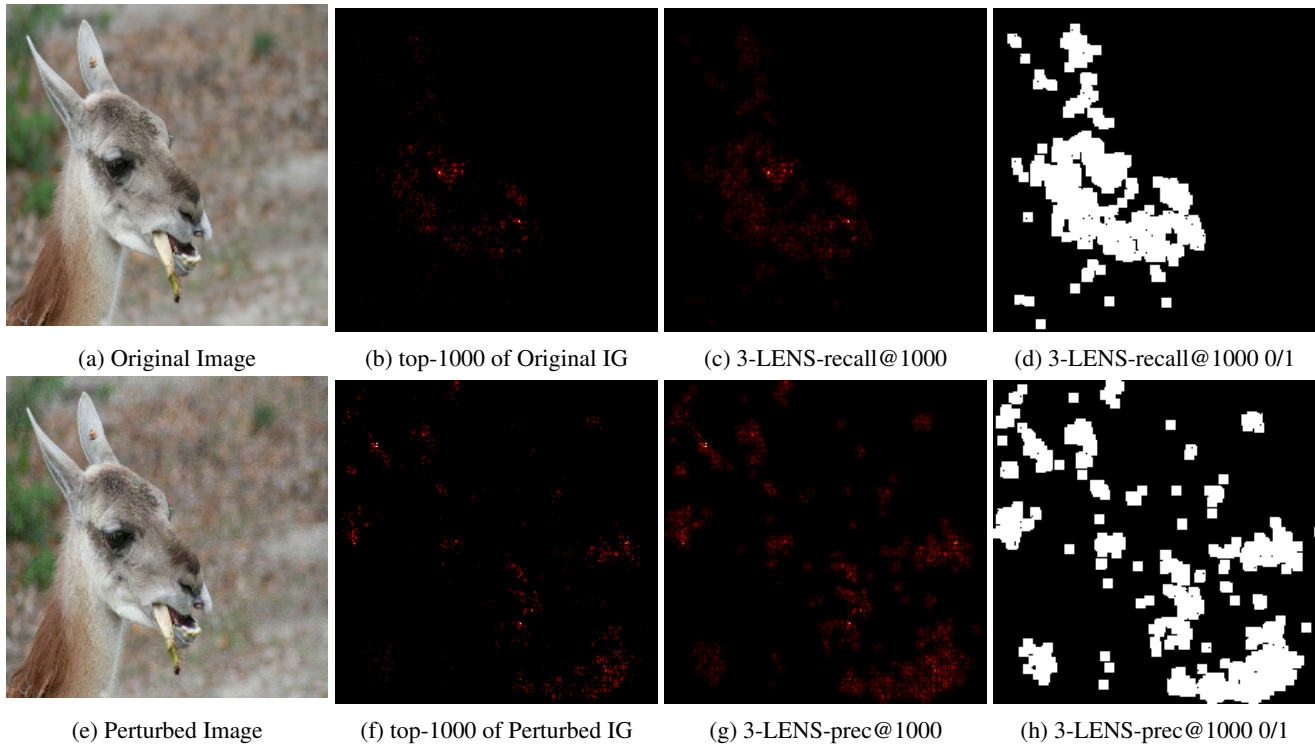


Figure 36: Example based on locality(LENS) with sample Integrated Gradients(IG) map from ImageNet dataset (a) the original image and (b) being the perturbed image. (c) and (d) show top- k highlighted and (e) and (f) are the corresponding maps with LENS. Maps (g), (h) are the maps corresponding to (e), (f), respectively with non-zero value pixels shown as white. top- k :0.108, 3-LENS-recall@ k :0.254, 3-LENS-prec@ k :0.433, top- k -div:0.090, 3-LENS-recall@ k -div:0.758, 3-LENS-prec@ k -div:0.807

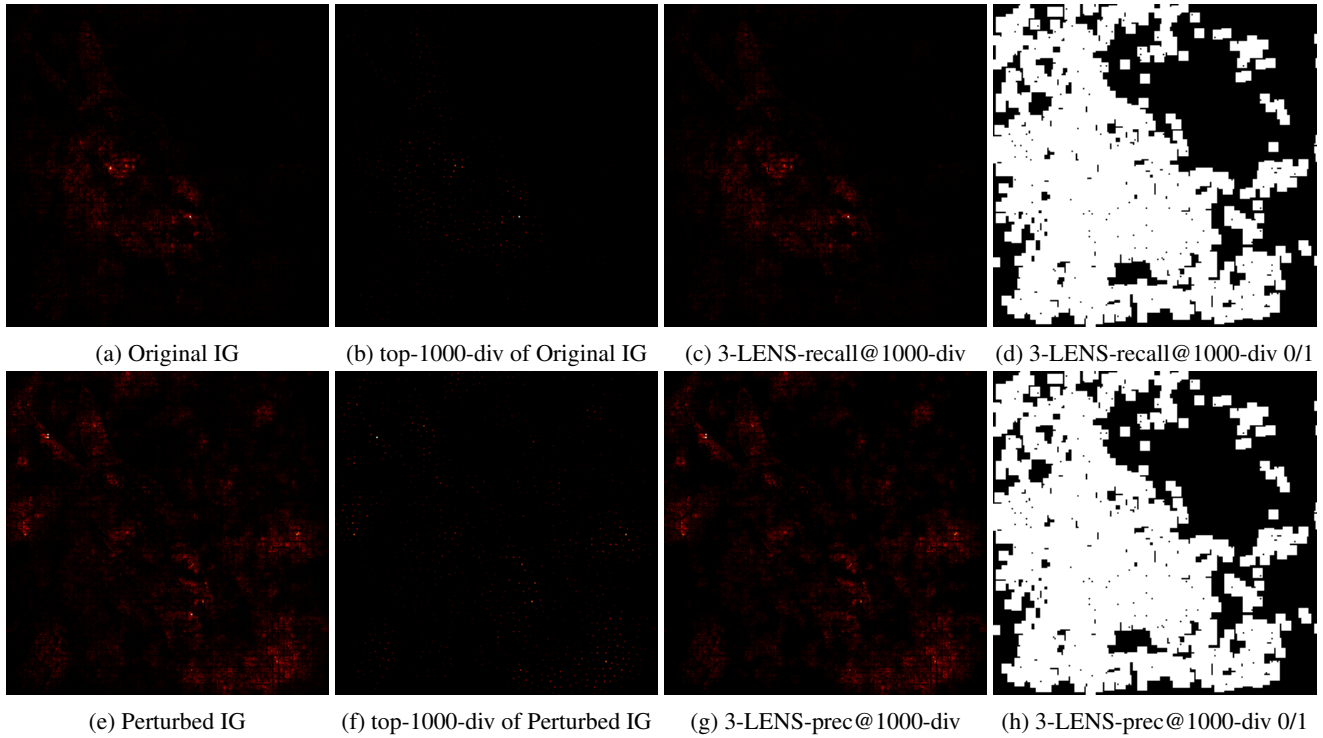


Figure 37: Example based on diversity with 7×7 window size with sample Integrated Gradients(IG) map from ImageNet dataset (a) the original IG of unperturbed image and (b) perturbed IG obtained with top- k attack(Ghorbani, Abid, and Zou 2019). (c) and (d) show top- k -div highlighted and (e) and (f) are the corresponding maps with LENS. Maps (g), (h) are the maps corresponding to (e), (f), respectively with non-zero value pixels shown as white. top- k :0.108, 3-LENS-recall@ k :0.254, 3-LENS-prec@ k :0.433, top- k -div:0.090, 3-LENS-recall@ k -div:0.758, 3-LENS-prec@ k -div:0.807

G Additional results for PGD-trained and IG-SUM-NORM trained models

Figure 11 and Figure 12 shows the impact of k in top- k for adversarially(PGD) trained and attributional(IG-SUM-NORM) trained network, respectively. But an important point to be noticed is that even with small number of features LENS is able to cross 70-80% which supports the observation of sparsity and stability of attributions achieved by adversarially(PGD) trained models by Chalasani et al. (2020). Similarly, the experiments with different w value for w -LENS-top- k in Figure 19 clearly indicates that due to the stability properties at lower window sizes LENS is able to cross the 80% intersection quickly. Supporting that our metric nicely captures local stability very well.

While above we observed only the top- k version of LENS. Figure 14 further extends the observation to LENS-Spearman and LENS-Kendall who to show that with LENS with a smoothing of 3×3 the maps from PGD-trained and IG-SUM-NORM trained models have a higher top- k intersection above 70% in comparison to natural trained model across all datasets used in our experiments, which further strengthen the conclusions from previous papers that IG on PGD-trained and IG-SUM-NORM trained models give better attributions.

Appendix E and H provide results on PGD-trained and IG-SUM-NORM trained models along with naturally trained models for compact presentation of results.

H Additional results with top- k -div

Table 4 provides detailed LENS and diversity with LENS results on MNIST, Fashion-MNIST, Table 5 on Flower with natural, PGD and IG-SUM-NORM trained networks and Table 6 on naturally trained network for ImageNet. All results with top- k , center of mass attack proposed by Ghorbani, Abid, and Zou (2019) and random sign perturbation using Integrated Gradients(IG).

Table 7 show the LENS and diversity results with random sign perturbation on MNIST, Fashion MNIST and Table 8 on ImageNet with different explanation methods like Simple Gradients(SG), Image \times Gradient, DeepLIFT(Shrikumar et al. 2016; Shrikumar, Greenside, and Kundaje 2017), LRP (Bach et al. 2015), GradShap(Lundberg and Lee 2017) and Integrated Gradients(IG) (Sundararajan, Taly, and Yan 2017).

Dataset	Train Type	Attack Type	Attribution Method	top- k intersection	1-LENS-recall@ k	1-LENS-prec@ k	top- k -div	1-LENS-recall@ k -div	1-LENS-prec@ k -div
MNIST	Nat	top- k	IG	0.4635	0.6209	0.9427	0.1680	0.6592	0.8126
	Nat	mass center	IG	0.5779	0.7146	0.9572	0.1708	0.6183	0.7191
	Nat	random	IG	0.7384	0.8790	0.9808	0.2046	0.6774	0.8140
MNIST	PGD	top- k	IG	0.5378	0.6127	0.9690	0.2300	0.6567	0.8114
	PGD	mass center	IG	0.6077	0.7133	0.9700	0.1907	0.5894	0.6801
	PGD	random	IG	0.6867	0.8220	0.9835	0.1751	0.6726	0.7995
MNIST	IG-SUM-NORM	top- k	IG	0.6406	0.7817	0.9736	0.2327	0.6701	0.7995
	IG-SUM-NORM	mass center	IG	0.7075	0.8387	0.9695	0.2002	0.6293	0.7294
	IG-SUM-NORM	random	IG	0.7746	0.9129	0.9846	0.1783	0.6788	0.8142
Fashion-MNIST	Nat	top- k	IG	0.3841	0.9118	0.9361	0.2132	0.8404	0.8857
	Nat	mass center	IG	0.5624	0.9333	0.9370	0.2961	0.8034	0.8277
	Nat	random	IG	0.5378	0.9377	0.9500	0.2716	0.8337	0.8825
Fashion-MNIST	PGD	top- k	IG	0.7440	0.9571	0.9696	0.3770	0.8486	0.8608
	PGD	mass center	IG	0.8543	0.9659	0.9721	0.4323	0.8249	0.8357
	PGD	random	IG	0.8816	0.9863	0.9892	0.3806	0.8451	0.8695
Fashion-MNIST	IG-SUM-NORM	top- k	IG	0.6953	0.9608	0.9697	0.3671	0.8437	0.8655
	IG-SUM-NORM	mass center	IG	0.8630	0.9666	0.9752	0.4485	0.8278	0.8437
	IG-SUM-NORM	random	IG	0.8733	0.9837	0.9900	0.3459	0.8444	0.8766

Table 4: Table with top- k intersection and top- k -div results for MNIST and Fashion MNIST with LeNet based model using Integrated Gradients(IG) (Sundararajan, Taly, and Yan 2017). The columns first contain locality results: top- k intersection, 1-LENS-recall@ k , 1-LENS-prec@ k followed by diversity results: top- k -div, 1-LENS-recall@ k -div, 1-LENS-prec@ k -div. Models trained naturally, PGD and IG-SUM-NORM are used. Results include top- k , center of mass attack of Ghorbani, Abid, and Zou (2019) as well as random sign perturbation.

Dataset	Train Type	Attack Type	Attribution Method	top- k intersection	2-LENS-recall@ k	2-LENS-prec@ k	top- k -div	2-LENS-recall@ k -div	2-LENS-prec@ k -div
Flower	Nat	top- k	IG	0.1789	0.4091	0.5128	0.2355	0.9482	0.9560
	Nat	mass center	IG	0.4248	0.7196	0.6664	0.2645	0.9360	0.9420
	Nat	random	IG	0.8206	0.9709	0.9747	0.4613	0.9741	0.9778
Flower	PGD	top- k	IG	0.5941	0.8444	0.9165	0.4078	0.9733	0.9737
	PGD	mass center	IG	0.6983	0.9223	0.9303	0.4247	0.9656	0.9655
	PGD	random	IG	0.9033	0.9929	0.9934	0.5948	0.9847	0.9886
Flower	IG-SUM-NORM	top- k	IG	0.6179	0.8720	0.9299	0.3875	0.9747	0.9757
	IG-SUM-NORM	mass center	IG	0.7053	0.9303	0.9435	0.4031	0.9667	0.9672
	IG-SUM-NORM	random	IG	0.8874	0.9917	0.9927	0.5707	0.9841	0.9869

Table 5: Table with top- k intersection and top- k -div results for Flower with ResNet based model using Integrated Gradients(IG) (Sundararajan, Taly, and Yan 2017). The columns first contain locality results: top- k intersection, 2-LENS-recall@ k , 2-LENS-prec@ k followed by diversity results: top- k -div, 2-LENS-recall@ k -div, 2-LENS-prec@ k -div. Models trained naturally, PGD and IG-SUM-NORM are used. Results include top- k , center of mass attack of Ghorbani, Abid, and Zou (2019) as well as random sign perturbation.

Dataset	Train Type	Attack Type	Attribution Method	top- k intersection	3-LENS-recall@ k	3-LENS-prec@ k	top- k -div	3-LENS-recall@ k -div	3-LENS-prec@ k -div
ImageNet	Nat	top- k	IG	0.0544	0.2822	0.3189	0.0684	0.7303	0.7458
	Nat	mass center	IG	0.0869	0.3994	0.2082	0.0914	0.7221	0.7114
	Nat	random	IG	0.3133	0.8463	0.8460	0.2157	0.8713	0.8689

Table 6: Table with top- k intersection and top- k -div results for ImageNet with SqueezeNet model using Integrated Gradients(IG) (Sundararajan, Taly, and Yan 2017). The columns first contain locality results: top- k intersection, 3-LENS-recall@ k , 3-LENS-prec@ k followed by diversity results: top- k -div, 3-LENS-recall@ k -div, 3-LENS-prec@ k -div. Models naturally trained are used. Results include top- k , center of mass attack of Ghorbani, Abid, and Zou (2019) as well as random sign perturbation.

Dataset	Train Type	Attack Type	Attribution method	top- k	1-LENS-recall@ k	1-LENS-prec@ k	top- k -div	1-LENS-recall@ k -div	1-LENS-prec@ k -div
MNIST	Nat	random	Simple Gradient	0.6548	0.8872	0.9355	0.2431	0.8724	0.8942
	Nat	random	Image \times Gradient	0.6887	0.8590	0.9791	0.1640	0.6725	0.7735
	Nat	random	LRP [Bach 2015]	0.6887	0.8590	0.9791	0.1640	0.6725	0.7733
	Nat	random	DeepLIFT [Shrikumar 2017]	0.6896	0.8602	0.9792	0.1642	0.6725	0.7724
	Nat	random	GradSHAP [Lundberg 2017]	0.6950	0.8629	0.9792	0.1646	0.6716	0.7707
	Nat	random	IG [Sundararajan 2017]	0.6978	0.8636	0.9795	0.1654	0.6717	0.7705
MNIST	PGD	random	Simple Gradient	0.4456	0.7544	0.9712	0.1798	0.8034	0.8719
	PGD	random	Image \times Gradient	0.5355	0.8102	0.9853	0.1620	0.6788	0.8037
	PGD	random	LRP [Bach 2015]	0.6887	0.8590	0.9791	0.2786	0.8669	0.9557
	PGD	random	DeepLIFT [Shrikumar 2017]	0.5387	0.8111	0.9855	0.1626	0.6795	0.8056
	PGD	random	GradSHAP [Lundberg 2017]	0.6831	0.9164	0.9835	0.1611	0.6684	0.7619
	PGD	random	IG [Sundararajan 2017]	0.6729	0.9359	0.9847	0.1671	0.6641	0.7573
Fashion-MNIST	Nat	random	Simple Gradient	0.5216	0.8421	0.8614	0.2691	0.8718	0.8820
	Nat	random	Image \times Gradient	0.5840	0.9160	0.9317	0.2570	0.8357	0.8719
	Nat	random	LRP [Bach 2015]	0.5840	0.9160	0.9317	0.2570	0.8357	0.8719
	Nat	random	DeepLIFT [Shrikumar 2017]	0.5821	0.9165	0.9311	0.2560	0.8370	0.8716
	Nat	random	GradSHAP [Lundberg 2017]	0.6075	0.9208	0.9377	0.2641	0.8391	0.8717
	Nat	random	IG [Sundararajan 2017]	0.6279	0.9281	0.9443	0.2736	0.8387	0.8713
Fashion-MNIST	PGD	random	Simple Gradient	0.6036	0.8374	0.9362	0.2974	0.8202	0.8696
	PGD	random	Image \times Gradient	0.6561	0.9236	0.9648	0.3118	0.8472	0.8820
	PGD	random	LRP [Bach 2015]	0.6561	0.9236	0.9648	0.3118	0.8472	0.8820
	PGD	random	DeepLIFT [Shrikumar 2017]	0.6628	0.9255	0.9662	0.3124	0.8496	0.8838
	PGD	random	GradSHAP [Lundberg 2017]	0.6678	0.9428	0.9625	0.3023	0.8573	0.8723
	PGD	random	IG [Sundararajan 2017]	0.7103	0.9638	0.9809	0.3242	0.8583	0.8751

Table 7: Table with top- k intersection and top- k -div results for MNIST and Fashion MNIST with LeNet based model trained naturally and adversarially(PGD), using different explanation methods with random sign perturbation. The columns first contain locality results: top- k intersection, 1-LENS-recall@ k , 1-LENS-prec@ k followed by diversity results: top- k -div, 3-LENS-recall@ k -div, 3-LENS-prec@ k -div.

Dataset	Train Type	Attack Type	Attribution method	top- k	3-LENS-recall@ k	3-LENS-prec@ k	top- k -div	3-LENS-recall@ k -div	3-LENS-prec@ k -div
ImageNet	Nat	random	Simple Gradient	0.3825	0.7875	0.7949	0.3096	0.8290	0.8115
	Nat	random	Image \times Gradient	0.3316	0.7765	0.8134	0.2905	0.8655	0.8516
	Nat	random	LRP [Bach 2015]	0.1027	0.2487	0.2649	0.0970	0.7518	0.7371
	Nat	random	DeepLIFT [Shrikumar 2017]	0.2907	0.7641	0.7637	0.2547	0.8504	0.8578
	Nat	random	GradSHAP [Lundberg 2017]	0.2290	0.6513	0.6778	0.1885	0.8099	0.7979
	Nat	random	IG [Sundararajan 2017]	0.2638	0.7148	0.7064	0.2366	0.8380	0.8296
ImageNet	PGD	random	Simple Gradient	0.1725	0.7245	0.7306	0.1410	0.8004	0.8004
	PGD	random	Image \times Gradient	0.1714	0.7269	0.8043	0.1332	0.8552	0.8687
	PGD	random	LRP [Bach 2015]	0.2374	0.4147	0.4350	0.1240	0.8161	0.8210
	PGD	random	DeepLIFT [Shrikumar 2017]	0.5572	0.9746	0.9808	0.2924	0.8977	0.9078
	PGD	random	GradSHAP [Lundberg 2017]	0.1714	0.7270	0.8044	0.1336	0.8552	0.8688
	PGD	random	IG [Sundararajan 2017]	0.1947	0.7335	0.8036	0.1524	0.8584	0.8696

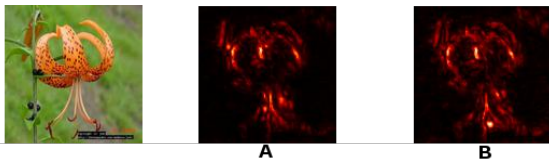
Table 8: Table with top- k intersection and top- k -div results for ImageNet with naturally and adversarially(PGD) trained ResNet50 model using different explanation methods with random sign perturbation. The columns first contain locality results: top- k intersection, 1-LENS-recall@ k , 1-LENS-prec@ k followed by diversity results: top- k -div, 3-LENS-recall@ k -div, 3-LENS-prec@ k -div.

I Details of Survey Conducted to Study Human’s Perception of Robustness

Detailed description of the survey conducted to study human’s interpretation of attribution maps.

Survey Format: Each question consisted of an unperturbed image from the Flower dataset and a pair of explanation/attribution maps. The pair can be any combination of original and attribution map obtained with random perturbation or with Ghorbani, Abid, and Zou (2019) attack. We used Integrated Gradients (IG) (Sundararajan, Taly, and Yan 2017) to obtain the attribution maps. Perturbed maps were obtained using the Ghorbani, Abid, and Zou (2019) attack and random noise with appropriate ϵ -budget. The questions were presented at random. At no point in the survey we revealed the type of map or perturbation added to obtain the maps. This ensured the user was not biased by this extra information while answering the survey. A sample question presented to the user is as given below :

Here is an image of **Tigerlily** with two attribution maps.



Do both these attribution maps explain the image well?

- (1) Yes, both are similar and explain the image well.
- (2) Yes, both explain the image well, but are dissimilar.
- (3) Only A explains the image well, B is different.
- (4) Only B explains the image well, A is different.
- (5) No, Both the maps do not explain the image well.

Interpretation of Options: Options (1), (2) the user is able to relate both the maps to equally represent the image. Option (3) the user finds map A to represent the image over map B. Option (4) the user finds map B relates to the image more closer than map B. Option (5) the user can not relate the maps to the image.

Table 1 in the main paper, we simplify the options by forming 2 categories - (1) **Agree with 3-LENS-prec@k metric** : combines Option (1), (2) and (4). These options show that the top- k metric does not match human visual perception when the user either is agnostic to noise in the map or finds the perturbed map more relatable to the image. (2) **Agree with top- k metric** : Only Option (3). It shows that top- k metric is sufficient to measure the differences between the attribution maps and closely captures human visual perception.

Summary of Survey Results: In the above sample question, map **A** is the original IG map of the image and map **B** the IG map of Ghorbani, Abid, and Zou (2019) attacked image with $\epsilon = 8/255$. Interestingly the users who chose between (1) to (4), more than 65% users chose option (1), (2) or (4) (Agree with 3-LENS-prec@ k metric), while remaining preferred option (3) (Agree with top- k metric). Showing that

despite the top- k intersection being less the 30% between the maps, users who fall into the **Agree with 3-LENS-prec@ k metric** category is large indicating that current top- k based comparison is weak.

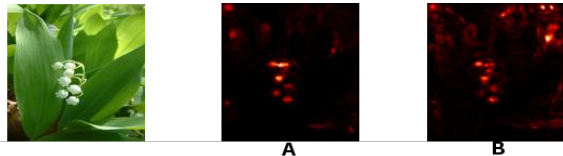


Figure 38: Sample question from survey using **Lily Valley** image with original IG map and IG map with Ghorbani, Abid, and Zou (2019) attack using $\epsilon = 8/255$.

In another sample from the survey (Figure 38), surprisingly more the 50% who fall in the category **Agree with 3-LENS-prec@k metric** preferred the perturbed map over the original map. top- k and 3-LENS-prec@ k values were 36% and 88%, respectively.

We did have few questions in the survey to study the effectiveness of random perturbation as an attack as observed by Ghorbani, Abid, and Zou (2019)[Figure 3] with top- k metric. We used $\epsilon = 8/255$ for the random perturbation. The results of the survey were very unanimous with users responses overwhelmingly(above 90%) fell into the **Agree with 3-LENS-prec@k metric**. This strongly indicates that random perturbation considered as an attack under current metrics gives a false sense of attribution robustness. Refer to the last entries in Table 9.

Attack Type	Agree with 3-LENS-prec@k metric(%)	Agree with top-k metric(%)	top-1000 intersection	3-LENS-prec@1000
top-k	70.37	29.63	0.343	0.928
top-k	81.48	18.52	0.0805	0.521
random	93.55	6.45	0.357	0.7965

Table 9: Survey results based on humans ability to relate the explanation map to the original image with or without noise using the Flower dataset using Integrated Gradients (IG) (Sundararajan, Taly, and Yan 2017) as the explanation method.